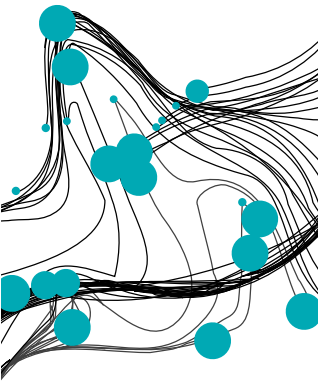

RAM ROBOTICS AND MECHATRONICS

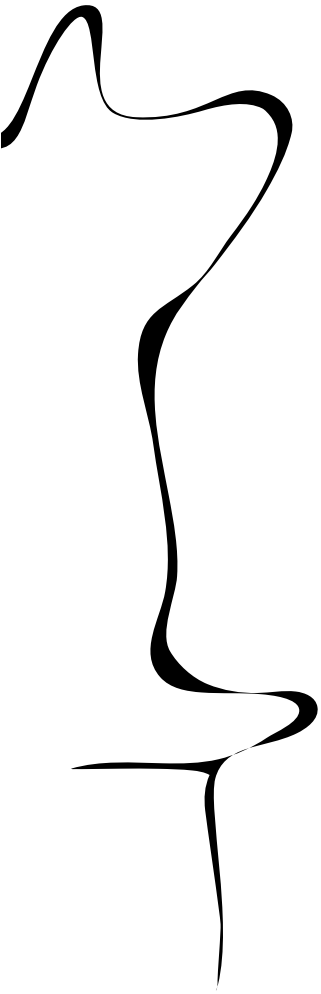

AERIAL MANIPULATION OF DEFORMABLE OBJECTS

V.B. (Vignesh Balaji) Vijayan

MSC ASSIGNMENT

Committee:
prof. dr. ir. A. Franchi
C. Gabellieri, Ph.D
dr. I.S.M. Khalil

August, 2024

059RaM2024
Robotics and Mechatronics
EEMCS
University of Twente
P.O. Box 217
7500 AE Enschede
The Netherlands

UNIVERSITY OF TWENTE. | TECHMED CENTRE UNIVERSITY OF TWENTE. | DIGITAL SOCIETY INSTITUTE

Abstract

This work presents a novel modeling method designed for the control of multiple quadrotors carrying a net, modeled as cables, to collect litter from water bodies. This method addresses the limitations of conventional litter collection approaches, such as the use of boats, which are ineffective in non-navigable areas like lagoons and streams. These problems are overcome with the capabilities of aerial manipulation. This research extends the state-of-the-art in modeling methods used for control algorithms in aerial manipulation. The validity of the proposed modeling approach and its underlying assumptions were experimentally tested, with metrics evaluated to ensure accuracy. A suitable simulation environment was developed by comparing three existing methodologies, and the most suitable and modular framework was chosen and implemented as a simulation framework to simulate the system. This work is a part of Flyflic (FLYing companion for Floating LItter Collection) project.

Acknowledgements

I would like to thank Professor Antonio Franchi and Chiara Gabellieri for giving me the opportunity to work in the research group. The Brainstorming meetings and the Action learning meetings increased my interest in the aerial robotics research field. I thank Professor Antonio franchi for helping me with opportunities for both my internship and thesis, his open feedbacks and insights helped me develop and grow. I thank my daily supervisor chiara gabellieri with whom i had many interesting and stimulating discussions. Her support and help made me progress. This also helped me to stimulate my interests. Her insights of breaking the problem down helped me to solve them. I thank her for all the help, understanding approach, flexibility and support for me in the difficult times.

I thank Prof.Islam for his kind gesture of accepting to be my external supervisor. I remember the interesting and understanding conversations we had during the courses and about the project. I thank Yaolei Shen for all the inspiring conversation we had about the project and about robotics research. His friendly approach helped me to discuss many problems and understand the importance of having physical intuition and insights. I like to thank my friends Ananth, Bhanu, Catia, Ahmed and Dimitris for their interesting conversations and help.

I would like to thank Jolanda for all her help and kindness towards me. I like to thank my mother, father, brother and relatives without whose support, I wouldn't be the person who i am today. Their constant belief and support helped me to travel towards my goals. I thank everyone who helped me in this journey. I am very happy to have had the opportunity to experience research. It has been a long standing dream from my childhood.

Abbreviations

UAV	Unmanned Aerial Vehicles
MRAV	Multi Rotor Aerial Vehicles
MAV	Micro Aerial Vehicles
AR	Aerial Robot
AM	Aerial Manipulation
VTOL	Vertical Takeoff and Landing
DoF	Degree of Freedom
DLO	Deformable Linear Object
DOM	Deformable Object Manipulation
Flyflic	Flying companion for floating litter collection
ANET	Aerial NET
SDF	Simulation Description Format
URDF	Unified Robotic Description Format
XML	Extensible Markup Language
XACRO	XML Macros
ERB	Embedded Ruby
ROS1	Robot Operating System version 1
ROS2	Robot Operating System version 2
MPC	Model Predictive Controller
LMPC	Linear Model Predictive Controller
NMPC	Non Linear Model Predictive Controller
OCP	Optimal Control Problem
QP	Quadratic Programming
APhI	Aerial Physical Interaction
RAM	Robotics and Mechatronics Laboratory
CW	Clock Wise
CCW	Counter Clock Wise
CoM	Centre Of Mass
CoG	Centre Of Gravity
AAU	Atomic Actuation Unit
1D	1-dimensional
2D	2-dimensional
3D	3-dimensional

Notations

$\mathcal{F}_W$	Inertial World Fixed Frame
$\mathcal{F}_B$	Moving Body Frame attached to CoM
τ	torque
F	Force
u_v	Tilting Angle of Propellers
u_λ	Control Inputs
N	Number of AU (or) Propellers
J	Inertia Matrix
$SO(3)$	Special Orthogonal group 3
$SE(3)$	Special Euclidean group 3
$S(2)$	Representing a surface
$S(3)$	Representing a sphere
$\mathbb{R}$	1 dimensional vector space
$\mathbb{R}^2$	2 dimensional vector space in 2x1 Matrix
$\mathbb{R}^3$	3 dimensional vector space in 3x1 Matrix
$\mathbb{R}^{3\times3}$	Real number 3x3 Matrix
a	Slope of the catenary curve (or) catenary number
x_0	Horizantal axis value of lowest point (or) symmetry point in a catenary curve
b	Vertical axis value of lowest point (or) symmetry point in a catenary curve
L	Length of a catenary curve
d	Horizontal distance between 2 end points of a catenary curve
v	Vertical distance between 2 end points of a catenary curve

Contents

List of Figures

List of Tables

1 Introduction

The interest in Aerial Robots (AR) started in 1903 right after Wright brothers invented a successful airplane. After that many people started working on different kinds of aerial platforms for increasing the ease of construction, mobility and maneuverability. The ease of maneuverability increases in Vertical Take Off and Landing (VTOL) platforms and attempts were made to construct multi-rotor vehicles for this application.

The use of multi-rotors were preferred compared to single main rotor and a tail rotor, similar to nowadays helicopter design is because the tail rotor proved to be inefficient consuming more power (around 15 % total power). Hence, multi-rotor design were preferred as all the rotors were used to generate lift.

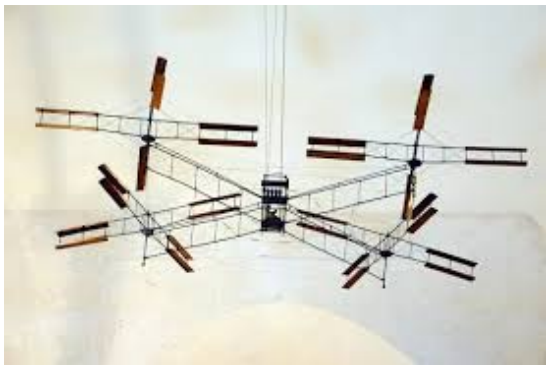

(a) A miniature version of the first quadrotor (gyroplane 1) in paris museum, original version built by Jacques in 1907 [23]

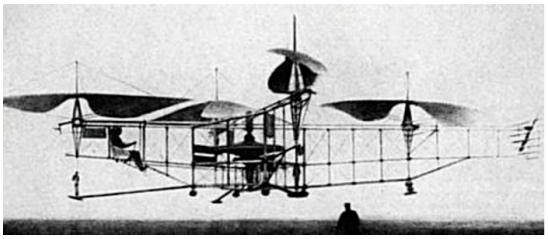

(b) The real working Oehmichen quadrotor in a manned test flight in 1924, showed the first operational experiment of a multi-rotor [36]

(c) The real working Bothezat quadrotor for the US army around 1924 [24]

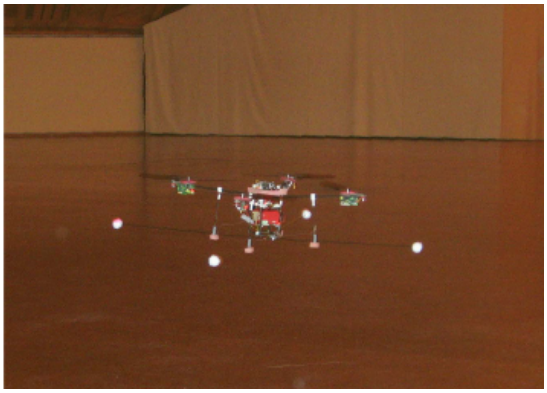

(d) A first working autonomous mini-quadrotor called OX4 in successful experiment in 2007 [8]

Figure 1.1: The transformation of Multi-Rotor Aerial Vehicle from invention to current state of the art

In 1907, Jacques and Louis breguet developed the first multi-rotor VTOL (quadcopter) figure 1.1a. Although, it was unstable and mechanically complex it laid the foundation for subsequent multi-rotor platforms. In 1924, Etienne Oehmichen designed a stable manned quadcopter called Oehmichen 2 and it travelled for 360 meters figure 1.1b . Around the same time, George de Bothezat did flight tests for US army for a similar platform named Bothezat quadcopter figure 1.1c and was able to hover at a maximum of 5 meters.

The stability of these platforms were bad as they are not naturally stable and increased the workload of the pilots. This made them to pivot to current helicopter of designs (with natural stability and less efficiency) for next few decades. This changed after the invention of computers and good electric motors which made the construction and control of multi-rotors (eg:- quadrotors) much easier com-

pared to single rotors. This is because in single main rotor designs, the pitch needs to be controlled whereas in multi-rotors only the speed/ rotations per minute (rpm) of the individual rotors needs to be corrected [36]. Due to the latest developments in computation, completely autonomous quad-rotors of varies sizes were developed enabling new range of tasks and field in robotics as shown in figure 1.1d.

The applications with multi-rotors started by integrating different kinds of sensors like camera, infra-red (IR), lidar etc relating to inspection and surveillance. The maneuverability and unlimited work-space was very tempting to be used for contact based inspections for non-destructive testing [16] [22] . The success in aerial physical interaction and contact opened up a wide range of applications. Soon, new designs of MRAV's were continuously developed and tested with different number and configuration of the rotors as shown in figure 1.3.

Figure 1.2: Different Multi-rotor aerial platforms built in Multi-Robot Systems (MRS) research group as shown in [4]

Soon, the size of the Multi-Rotor Aerial Vehicle (MRAV) started becoming a constraint for the possible range of tasks. This required the need to built bigger and heavier custom MRAV plaforms as seen in figure 1.2 and 1.3 . Inorder to overcome this, collaborative MRAV were used to work on tasks involving heavier object manipulation as well objects requiring actuation at multiple points (eg:- long bars, platform etc). In this way, commonly available MRAV platforms can be used for different kinds of applications.

Figure 1.3: Different Multi-rotor aerial platforms with rotor tilt mechanisms for full actuation as shown in [29]

Hence, the research in co-operative aerial manipulation with MRAV's started to gain more interest. It was most commonly used for transportation of heavier rigid objects as shown in figure 1.4. The possible target applications mostly involved in industrial applications, construction applications, payload delivery applications etc. In this way, MRAVs are beginning to be used in real-world applications.

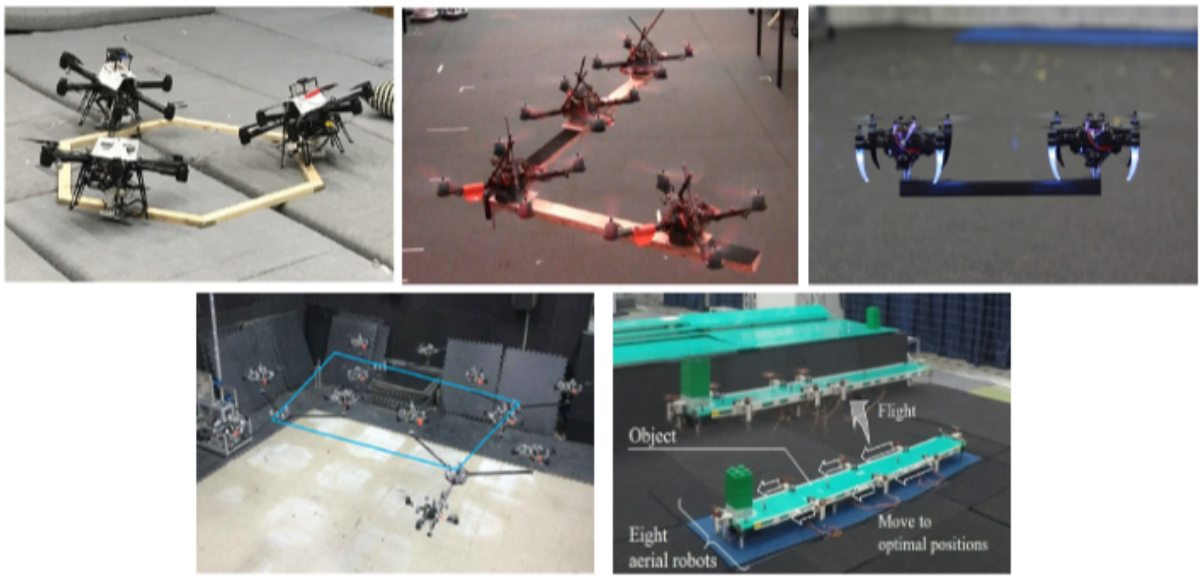

Figure 1.4: Different works of co-operative aerial transportation of rigid objects shown as a survey in [6]

1.1 Motivation

The MRAVs advantages like low cost, compact structure, agility, maneuverability etc was very promising to use it for other wide range of applications. This versatility helps to attain a larger workspace that conventional robots find it hard to attain. Since the current robotic applications has come more and more close to everyday human tasks. The superior capabilities of MRAVs were used to perform physical interaction with the environment by attaching manipulators to them. This kind of Aerial Manipulation (AM) can be used in complex environments that are inaccessible and unsafe for human workers. For example, testing wear and tear of wind mills, gas pipelines, fixing and maintenance of overhead high voltage electrical lines, assembly and disassembly of mechanical components at higher altitudes, installation of dividers, transportation of heavier objects at higher altitudes etc. Hence, Aerial Physical Interaction (APhI) is a rapidly developing field.

The additional degrees of freedom provided by aerial robots increases the possibilities of interacting with the environment at many constrained places and objects which are previously unreachable by ground and stationary robots. The MRAV's are the most suited type of AR for these type of tasks due to it's maneuverability capabilities. Based on the type of the interactions, it can be done by single or multiple MRAV's [39]. Inorder to achieve higher dexterity in operation and modularity of using existing platforms, Multi-robot (Multi-MRAV) co-operative systems are used for Aerial Physical Interaction (APhI).

In the recent years, there is active and extensive work on rigid body manipulation by MRAV's. The modelling methods for these types of robots were relatively easy due to the previous extensive work on rigid body manipulation. This mostly helped to build new models by using the pre-existing knowledge as building blocks for the new rigid body model of the whole system. The control methods need to be developed based on new changed model and dynamics of the system [5].

Everyday human tasks involves manipulating a lot of deformable objects apart from rigid bodies. Some of the deformable objects manipulation (DOM) includes clothes, foods, bags, charging cables, medical supplies etc. Every object has a deformability including the rigid bodies, but the level of deformability in rigid bodies is negligible.

The reason for difficulty of DOM is, the interaction forces cannot be easily summed up to produce a new displacement of the object. Depending upon the physical properties of the deformable object, a part of the interaction force is used for shape deformation and another part of interaction force is used for displacement of the object. Due to this, it requires changes in hardware design for grasping, sensing, modelling, planning and control. It requires changes in every stack of robotics to interact with deformable objects. Due to the these reasons the deformable objects manipulation (DOM) is non trivial. The fragility and difficulty in grasping adds to the complexity of DOM.

The deformable object manipulation (DOM) opens us manipulating objects for both position and shape dynamics by exploiting the properties of the system like elasticity. The modelling and control of these type of objects is not well studied due to the higher degrees of freedom of the objects and is in current active research. Hence, the work on any robot interacting with deformable and soft objects is relatively new and Aerial Robot (AR) involved in DOM is in it's nascent stage and has seen recent growth.

The initial works of DOM by Aerial Robots started with Deformable Linear Objects (DLO) such as cables, ropes, hoses etc. This is due to their one-dimensional simplicity compared to thin surface cloths (2-dimensional) and soft bodies (3-dimensional). The DLO's are one-dimensional, as they are mostly characterised by length, because the length is greater than width or thickness and the deformations usually involve stretching, bending a curve. Hence, DLO's are also called as deformable one-dimensional objects.

The easiest configuration to manipulate objects with DLO's (cables, ropes etc) is to keep them taut (fully extended due to tension, no slack). In this configuration DLO's can be treated as rigid bodies, only their tension forces and kinematic configuration is taken in the model. It is most commonly used for transportation of objects as shown in figure 1.5.

Inorder to manipulate the shape of the DLOs, the slackness of the DLOs (cables, ropes etc) need to be accounted. It helps in easily changing different configurations of the system, navigating in constrained environments etc.

1.2 Problem statement

The conventional method of litter collection from surface of water bodies include manual skimming with nets or rakes, using skimmer boats equipped with nets or vacuum systems, and deploying floating barriers that need regular manual cleaning. Most of these methods require human intervention within the water body or depend on navigable conditions suitable for traditional boats.

However, these methods are impractical in constrained water bodies such as rivers with steep gradients, streams, creeks, flooded quarries, wetlands, and moats. In these environments, human intervention is too hazardous, and the challenging conditions make it difficult or impossible to navigate with boats.

In these challenging scenarios, MRAVs (Multi-Rotor Aerial Vehicles) offer a viable solution. Their enhanced maneuverability allows them to access hard-to-reach and hazardous areas with ease. By equipping MRAVs with a collection net, they can efficiently gather litter, such as plastic, from the surface of water bodies. This system, can be referred as Aerial NET (ANET).

The system consists of a collecting net attached to multiple MRAVs, ideally 4, to hold each corner of the net as shown in figure 1.6. This setup allows for both manipulating the net's shape and position

Figure 1.5: Different works of co-operative aerial transportation objects using taut cables, shown as a survey in [6]

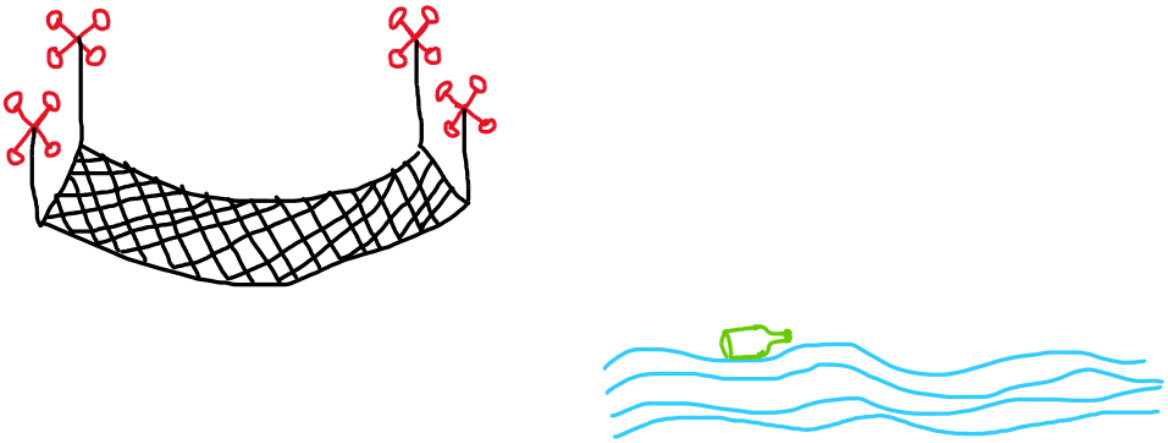

Figure 1.6: Pictorial representation of the configuration of the system and the intended application

in various configurations. For instance, the net can be fully stretched and can change different orientations to effectively gather litter from water bodies during collection maneuvers. Additionally, since the operating weight capacity of a single MRAV is limited, multiple MRAVs are employed to distribute the weight of the net and handle larger quantities of collected litter.

The modelling of the net is non trivial as it is a deformable object and encompass a large volume in 3-dimensional (3D) space. It is very hard to capture the deformation model of a 3D object, even capturing the deformation of a one-dimensional(1D) object or DLO is hard. Hence, a suitable model

needs to be identified which represents the system with respect to the intended application. The difficulty in selecting the model lies in the trade-off between the simplicity of the modelling approach and the efficiency of the model under different conditions. The different conditions include external disturbances like weight of the payload, water current on the net, wind gust etc.

1.3 Structure of report

The structure of the report is divided into 5 chapters. The main theme of each chapter is explained below.

- **Section I (Introduction)** - A brief about the related research field and about the problem statement
- **Section II (State Of the Art)** - Literature survey of the problem statement.
- **Section III (Modelling)** - The model used to represent the system and difficulties faced in modelling the system.
- **Section IV (Simulator)** - Different types of simulators used to simulate the system.
- **Section V (Discussion & Conclusion)** - Discussing about different methods and future directions.

1.4 Thesis Contribution

A simple and realistic way to model a net carried by multiple multi-rotors (quadrotors) was identified. The model and the assumptions used is the model is verified experimentally and the data is analaysed to validate the hypothesis. Three different ways to simulate the system is tried. The pros, cons and challenges were discussed and the most efficient model to be used for control purposes is suggested.

The thesis contribution can be explained by answering the 2 research questions -

1.4.1 Consider a system composed of multiple multirotors connected through deformable passive elements, such as cables. Identify a suitable model for such a system. The steps will be: a study of the literature on cable-connected aerial robotic systems; identification of a suitable model (simple yet realistic); and validation of the model

1.4.2 How to simulate such a system? Identify challenges, pros, and cons.

2 State of the Art

Different methods of simulating a deformable object is discussed in this chapter. The modelling method used in the project is chosen from one of the existing methods by keeping the tradeoff between simplicity and performance for a real time or onboard model.

2.1 Physics based models

It is a mathematical representation of the system based on the fundamental physical laws. Example:- Newton's laws of motion, conservation of energy etc. These models incorporate real world physical properties of the system like mass, force, friction etc.

2.1.1 Lumped parameters model

It is a simplification technique where the physical properties of the system like Mass, Stiffness, Damping etc are assumed to be uniformly distributed throughout as discrete components. This reduces the complexity of the system and makes it represent as a set of ordinary differential equations (ODEs).

Mass-Spring

It is the most commonly used modelling method for simulating deformable and soft bodies. This is because it represents the natural properties of the object. Every object, whether it is rigid or soft, can be represented as a combination of mass (M), stiffness or elasticity (K)and damping (D). If these parameters are accurately identified then it is possible to simulate any kind of object.

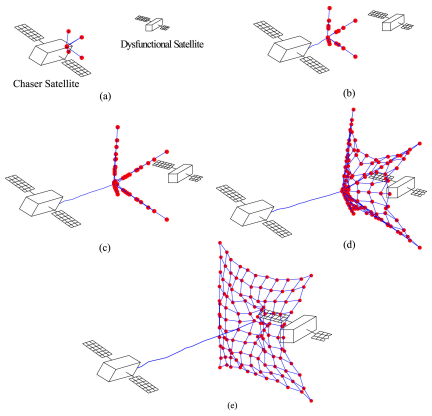

(a) The deployment dynamics of a net to remove space debris

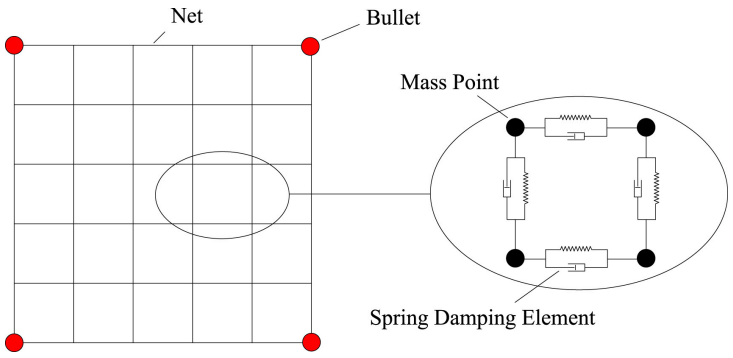

(b) The closeup view of the elements of a net

Figure 2.1: The application and the model of a collecting net [42]

This model also takes into consideration of discretisation of the object with these parameters of M,D and K. The level of discretization determines the level of deformability exhibited by the model. The level of discretization needed for a model is based on a number of factors like target application, computational intensity etc. The good part of modelling this way is it gives the dynamic model of the system. The benefit of this modeling approach is it gives the dynamic model of the system.

Most of the methods used to model a net includes a highly discretized model (very high dimensionality) of mass-spring-damper system, where numerous lumped masses are connected by parallel spring-damper elements, as shown in figures 2.1a and 2.1b. Due to the computational intensity of the model, it cannot be executed in real time or on-board and can only be done offline. This is not

suitable for machines like MRAVs which has on-board hardware constraints.

Additionally, simulating such a system offline while executing commands online presents its own set of challenges, much like sim-to-real transfer problems. This approach requires a detailed model of the target environment, and the complexity of that model increases significantly when physical interactions with the environment are necessary, as in this project.

Since it is very difficult to get an accurate model of the environment, having a simple and realistic model is very much preferred. Some efforts on this direction, involves using this modeling approach having a less discretized model, it will not give the complete deformation of the real world but still it could be very useful for specific constrained applications.

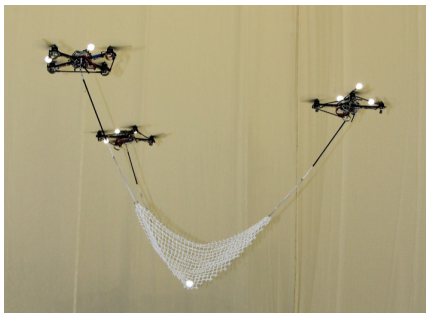

(a) The net is modelled as one mass connected by highly stiff springs to the quadrotors used for ball catching application [41]

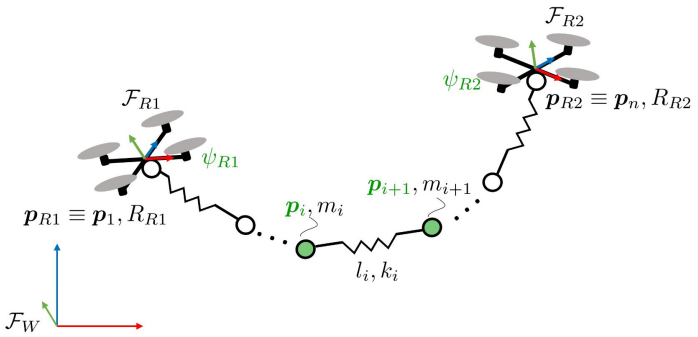

(b) The cable is modelled as 4 springs attached by 6 masses to manipulate 2 points in a cable [25]

Figure 2.2: Less discretized mass-spring systems used in aerial manipulation of deformable objects

For example, In [41] Yaohui et al, used one mass to represent the net and connected it with the 3 quadrotors with a high stiffness spring. It was useful to catch the ball only on the vertical plain. In [25] Chiara et al, used 5 springs and 6 masses to manipulate the position of 2 points in a cable connected to 2 quadrotors.

Rigid links

In the mass-spring model, the parameter identification and tunning of the parameters of M,D and K are difficult as it is mostly emprical. Inorder to remove this uncertainity, the lumped masses are connected to massless rigid links by spherical joints.

This modeling approach is effective for calculating the dynamics of deformable objects, but it does not consider the system's physical properties. As a result, behaviors such as stretching and compression are not captured. Additionally, the deformation dynamics of this model are influenced by its discretization, meaning the level of deformation is determined by the model's dimensionality.

In [27], goodarzi et al used this modelling approach to stabilise the system consisting of one quadrotor and a cable as shown in figure 2.3a. He used a geometric controller taking into account of the cable dynamics. In [30], kotaru et al showed used the property of differential flatness of the multi-quadrotor system carrying a load to plan feasible trajectories of the system as shown in figure 2.3b and tracked it using a LQR controller.

2.1.2 Distributed parameters model

Unlike the lumped parameters models in 2.1.1having discretization of physical parameters. The distributed parameters model are assumed to have a continuous variation of physical parameters over

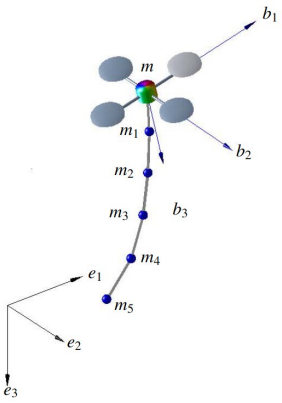

(a) Quadrotor with a single cable, modelled as many serial massless rigid links connected by spherical joints [27]

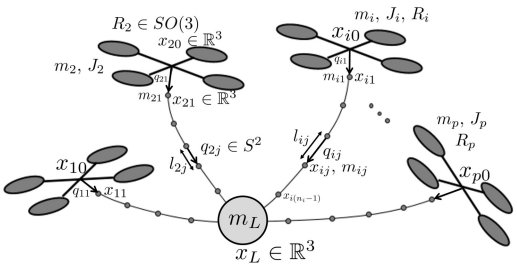

(b) Multi-quadrotors carrying a load connected by cables, modelled as many serial massless rigid links connected by spherical joints [30]

Figure 2.3: Discretized massless rigid link systems used in aerial manipulation of deformable objects

the entire system. This type of model can be represented by Partial Differential Equations (PDEs).

Distributed parameter systems are also called infinite-dimensional systems because the representation of the complete motion requires an infinite number of degrees. This is a highly accurate model compared to lumped parameters and are more computationally complex.

FEM & FDM

The Finite Element Method (FEM) and Finite Difference Method (FDM) are two most common methods used to solve Partial Differential Equations (PDEs). Both of them discretize the infinite dimensional (DoF) space in different ways. The FEM does it by breaking them into smaller finite elements like triangles, quadrilaterals etc. The FDM does it by approximating the derivatives of the PDE using finite differences method and thereby creating a grid for the entire domain space and approximating the derivatives at each grid point.

In [43], Yaolei et al used a partial differential equations (PDE) based model to represent a distributed parameter model for a quad-rotor carrying a cable and had boundary conditions based on ordinary differential equations (ODEs). It was used to do shape manipulation of the cable using a model based controller.

Beam Theory

The flexible and deformable objects can be modelled as beams. This allows to model the bending or flexibility of the object based on external forces applied to it (eg:-robot, environment etc) based on the properties of the system like young's modulus, density of the object, second moment of area and intersection area of the flexible load. This theory is also called as Euler-Bernoulli beam theory.

In [55],Hyunsoo et al used beam theory to manipulate the pose of flexible rod type using a collaborative movement between ground robot and aerial robot.

2.2 Geometric models

It is a mathematical way to describe the shape of a cable under the influence of different forces like gravity, external load etc. These techniques are mainly developed for structural analysis under

different loads and are currently used in robotics applications.

2.2.1 Parabola Model

It describes the shape of a flexible cable subjected to a uniformly distributed load along it's horizontal axis of the cable. It is primarily used for cables carrying an external load. This is because under normal conditions of a free hanging cable there is an error between the model and the actual cable, this error is less as the cable is horizontally stretched and this error is more when the two ends of the cable are near. For example, the error is directly proportional to the sag (slackness) of the cable. It is still a good approximation for certain configurations of the cable.

In [44], Lev et al modelled the shape of the cable as a parabola and used visual servoing to extract 3 features and track the velocities of the end points. In other words, the shape manipulation of a cable was performed as shown in figure 2.4a using a shape jacobian matrix.

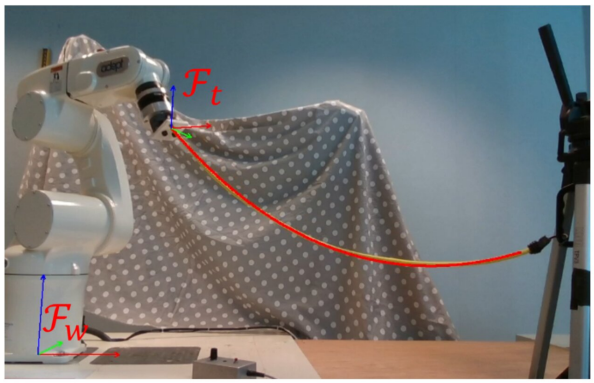

(a) Shape Manipulation of a cable using parabolic shape jacobian matrix [44]

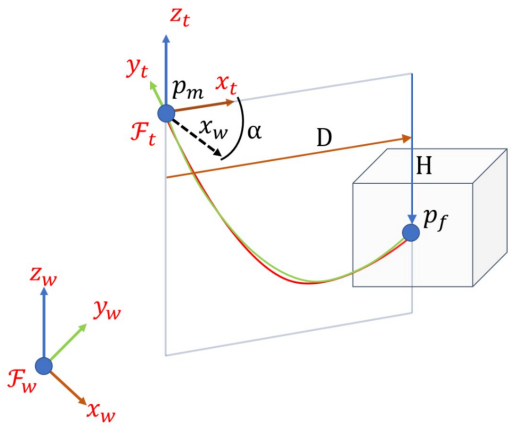

(b) The 3 parabolic features (yaw of plane, horizontal and vertical distance between end points) used in shape manipulation of cable [44]

Figure 2.4: Parabolic features used in shape manipulation of cable

2.2.2 Spline Model

It is used to control the shape and movement of a flexible cable by approximating the cable in the configuration space. It does it by diving the cable configuration into smaller segments between key point or control points and representing each deformation as a type of spline curve or a piece-wise polynomial curve.

The placement of the keypoints is related to the nature of the task. The number of key points determines the level of detail to represent the cable. The accuracy of the model is direactly proportional to the number of keypoints but it also increases the computational intensity of the system.

In [49], Tang et al comapred 2 methods of dividing the kepoints, Thin Plate Spline (TPS) and Tangent Space Mapping (TSM) between the key points. The results found that TSM is better than TPS as it is able to preserve the structural information of the cable such as length and shape between the shape deformation of the cable. The keypoints and the training simular is shown in figure 2.5a and 2.5b respectively.

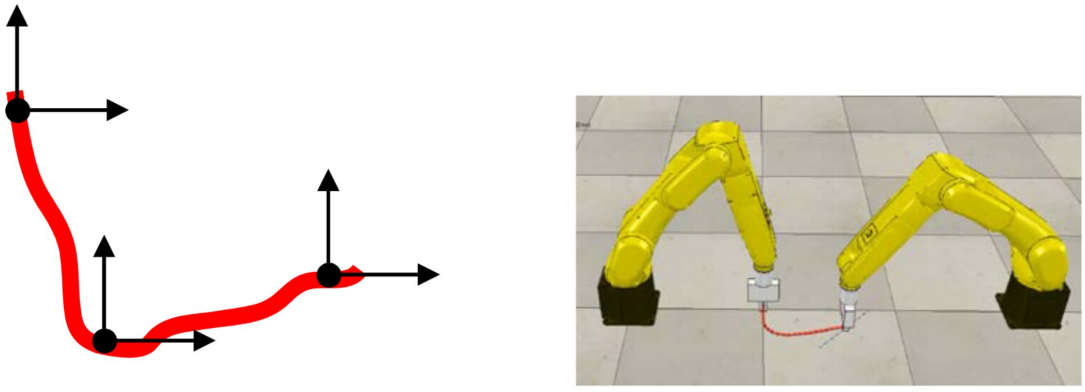

(a) The control or key points in a spline [49]

(b) Training tests for manipulation of cable [49]

Figure 2.5: Spline based model used for manipulation of a deformable cable

2.2.3 Catenary Model

The catenary perfectly describes the shape of a flexible and inextensible cable hanging under it's own weight supported at both of it's ends. The shape is formed due to the balance between cable tension forces and the gravitational force acting along the length of the cable. It assumes that the weight is uniformly distributed along the entire length of the cable, only gravitational force is acting on the cable and the cable is inextensible. The most important boundary condition is this shape holds only in static and quasi-static conditions.

There is a special branch of catenaries called elastic catenaries, it takes care of extensible catenaries. Since it considers the physical properties of the system and in this section we discuss geometric methods, only standard catenaries will be discussed in this section.

In [13], Diego et al used a catenary cable model propelled by 2 quadrotors and planned a trajectory to manipulate hook shaped objects and executed them by accounting for cable tensions as shown in figure 2.7a. In [20], Drupt et al estimated the shape of catenary cable in a neagtive buoyant environment (underwater) using Inertial measurement data generating local tangent angle at both of the cable to find other parameters of the catenary cable as shown in figure 2.7b. In [38], Martins et al used the tension of the cable based on catenary model to localise the quadrotor as shown in figure 2.7c. In [32], Laranjeira et al used visual servoing to control the tether shape deformation by attaching the end points of the tethers and moving them accordingly to manipulate the shapes as shown in figure 2.6d. The parameters of the tether are estimated by a non-linear least square fitting method.

In [21], Filliung et al added two additional degrees of freedom to represent the hydrodynamic effects such as sway, surge in the model. This model is tested for different kinds of materials in real world and a least square fit is evaluated between the theoretical model and the real world experiments. It established that this model is suited for dynamic motions of the cable and well suited for cable materials with negative boyancy.

The catenary is a one parameter DLO. The simplicity and effectiveness of the catenary based models was encouraging to do a detailed literature survey about the kind of works done in this way of modelling. The literature review is divided into two categories: the first covers the top level problem statement, while the second addresses the domain and the method used to solve the problem (e.g.,

(a) Manipulating hook shaped objects based on catenary model of cable with 2 quadrotors [13]

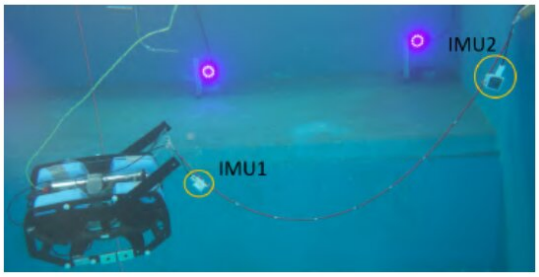

(b) Shape estimation of a catenary cable based on tangential angle from Interial Measurement Unit (IMU) data [20]

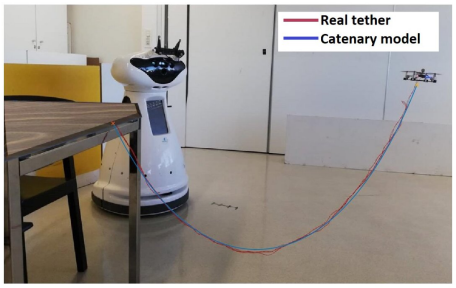

(c) Tension estimation and localisation of the quadrotor based on cable tension and it's parameters [38]

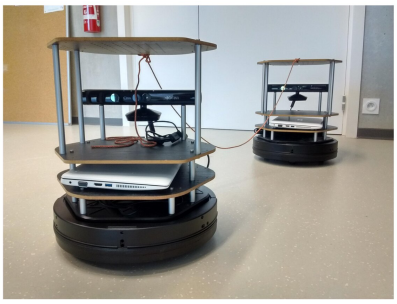

(d) Shape manipulation of a deformable cable based on visual servoing of a catenary based model [32]

Figure 2.6: Different catenary model based robots

controls, planning, system properties etc.).

In table 2.1, The literature survey is done based on types of problem statement approached with catenary based models.

Abbreviations used in table 2.1 -
sm - shape manipulation
ca - collision avoidance
uwsm - under water shape manipulation
mc - motion control
ct - cable tension
sew - analysis of static equilibrium with load
s - stability
fb - force based
kt - knot tying
ps - power supply

In table 2.2, The literature survey is done based on the methods (eg:- controls, planning used to solve the problem statement.

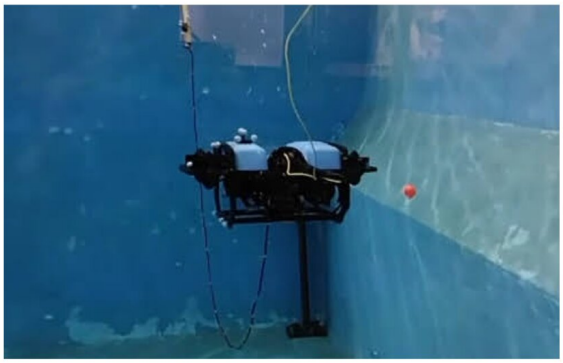

(a) Experimentation setup of test the shape estimation of different cables in under water, one end tied to support and other end operated by a remote operated vehicle [21]

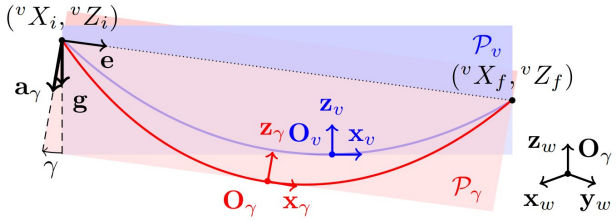

(b) An additional degree of freedom (angle) is used to represent the motion of the cable in a plane called as catenary plane. This is to represent the sway motion of the cable. This is shown by γ between the old position of catenary cable in a plane (purple) and new position of catenary cable in the plane (red) [21]

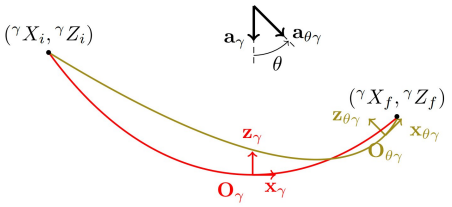

(c) Another degree of freedom is used to account for the in-plane motion of the cable, like surge motion. In the image, this is shown by θ between the previous position of cable (red) and the new position of cable (yellow). This angle changes perpendicular to the existing catenary plane. [21]

Figure 2.7: Augmented catenary model showing the representation of modified catenary model in the presence of hydrodynamic effects (eg:- sway and surge)

Table 2.2: Methodology used to solve the problem statements

References	Experiment	Problem Statement	Control Problem	Planning Problem	Properties
Deigo et al. 2021 [13]	✓	object manipulation with cables	geometric controller (feedforward ⊕ feedback) compensates cable tension and gravity	inverse kinematic planner	x
Ryan et al. 2019 [11]	✓	collaborative transport -fabric	Artificial potential (spring-damper, Lennard-Jones)	x	x
Vishal et al. 2021 [1]	x	vertical planar motion control 2 UAVs tethered with one end disturbance	state feedback ⊕ Extended high gain observer (disturbance)	x	feedback linearisation

Continued on next page

Table 2.2 – continued from previous page

References	Experiment	Problem Statement	Control Problem	Planning Problem	Properties
Ricardo et al. 2023 [38]	✓	tension estimation to quad (by IMU inertia, & motor thrust) ⊕ tether tension localisation	x	x	x
Marios et al. 2023 [45]	✓	2 tetherd UAVs fixed configuration path planning in confined environment	x	RRT for V shaped rigid body	x
Satoko et al. 2017 [2]	✓ pole and UAV (limited)	obstacle avoidance and shape estimation (no tension sensor)	PID feedback controller	x	x
Andrea et al. 2022[7]	✓	outdoor localisation (angle sensors at ends)	x	x	x
Deigo et al. 2022 [14]	x	knot tying withour re-grasping	x	knot theory	x
Deigo et al. 2021 [9]	x	planar co-operative transportation by wrapping and pulling (2 pair of catenary)	Adaptive Controller PD controller	x	x
Deigo et al. 2023 [12]	✓	forming hitch mid-air	x	motion primitives convex polygon	x
Xuesu et al. 2018 [54]	✓	tether based localisation	x	x	x
Kurt et al. 2018 [48]	x	static catenary parameters for heave robustness	x	x	x
Filliung et al. [21]	✓	Catenary with hydrodynamics	x	x	x
Chen et al. 2021 [35]	x	tether and stability, wind and landing phase	x	x	Lyapanov stability
Brendan et al. 2017 [26]	✓	considering catenary tension UAV motion	x	x	x

Continued on next page

Table 2.2 – continued from previous page

References	Experiment	Problem Statement	Control Problem	Planning Problem	Properties
Matheus et al. 2017 [32]	✓	sysetem identification tether torque model (inertia matrix roll,pitch)	x	x	x
Juliette et al. 2022 [20]	x	catenary shape negative buoyancy	x	x	x
Carlos et al. [51]	x	position reference planar VTOL	static state feedback ⊕ tension compensator	x	x
Martinez et al. 2021 [37]	x	collision free trajectory UAV-UGV tether	x	weighted multi-objective optimisation	x
Masaya et al. 2018 [47]	✓	position estimation by tensile force	x	x	transformation matrix analytical tension formulation
Federico et al. 2015 [3]	✓	pole - aerial knot tying	x	iterative policy gradient learning	x
Dimitris et al. 2022 [10]	x	stable flight inverse localisation from base to quad	back -stepping linearisation	x	x
Xuesu et al. 2019 [53]	✓	autonomous tethered UAV path execution	x	motion primitives for precomputed paths - 3 PID (position feedback) and inverse jacobian (model predictive feedforward velocity control)	x

Continued on next page

Table 2.2 – continued from previous page

References	Experiment	Problem Statement	Control Problem	Planning Problem	Properties
Rogerio et al. 2023 [33]	✓	3 tether based localisation (trignometric, catenary, neural network)	x	x	x
Rogerio et al. 2021 [34]	x	tether localisation (catenary equation and inertial data)	x	x	x
Miguel et al. 2009 [46]	x	multi-catenary analysis static equilibrium with point load	x	x	static equilibrium
Matheus et al. 2020 [31]	x	shape control in negative buoyancy (underwater)	leader - follower visual servoing	x	x
Seiga et al. 2017 [28]	✓	catenary localisation based sensor information	x	x	x
Sina et al. 2016 [19]	✓	catenary localisation (optimisation based)	x	x	x
Sigitas et al. 2013 [40]	x	stability analysis analysis tether and aerofoil $\oplus$ conditions stable equilibrium $\oplus$ wind disturbance	x	x	static catenary model augmented dynamic aerofoil $\oplus$ movement of equilibirum point for varying operating conditions

The above literature survey gave a detailed overview of the kind of problem and the approaches used for catenary based models.

Table 2.1: Literature survey on problem statements dealing with catenary based models

References	Object Manipulation	Transportation	Local	Disturbance Rejection	Multi Catenary	Net
Deigo et al. 2021 [13]	✓	✗	✗	✗	✗	✗
Ryan et al. 2019 [11]	✗	✓	✗	✗	✓	✗
Vishal et al. 2021 [1]	✗	✗	✓	✓	✗	✗
Ricardo et al. 2023 [38]	✗	✗	✓	✗	✗	✗
Marios et al. 2023 [45]	✗	✓	✗	✗	✗	✗
Satoko et al. 2017 [2]	✗	✓	✗	✗	✗	✗
Andrea et al. 2022 [7]	✗	✗	✓	✗	✗	✗
Deigo et al. 2022 [14]	✗	✓ sm	✗	✗	✓	✗
Deigo et al. 2021 [9]	✓	✓	✗	✗	✓	✗
Deigo et al. 2023 [12]	✗	✓ sm	✗	✗	✓	✗
Xuesu et al. 2018 [54]	✗	✗	✓	✗	✗	✗
Kurt et al. 2018 [48]	✗	✓ sm	✗	✓	✗	✗
Filliung et al. [21]	✗	✓ uwsm	✗	✓	✗	✗
Chen et al. 2021 [35]	✗	✓ s	✗	✗	✗	✗
Brendan et al. 2017 [26]	✗	✗	✗	✓ ct	✗	✗
Matheus et al. 2017 [32]	✗	✓ s	✗	✗	✗	✗
Juliette et al. 2022 [20]	✗	✓ uwsm	✗	✗	✗	✗
Carlos et al. 2021 [51]	✗	✓ ps	✗	✓ ct	✗	✗
Martinez et al. 2021 [37]	✗	✓ ca	✗	✗	✗	✗
Masaya et al. 2018 [47]	✗	✗	✓	✗	✗	✗
Federico et al. 2015 [3]	✗	✓ kt	✗	✗	✗	✗
Dimitris et al. 2022 [10]	✗	✗	✓ fb	✗	✗	✗
Xuesu et al. 2019 [53]	✗	✓ mc	✗	✗	✗	✗
Rogerio et al. 2023 [33]	✗	✗	✓	✗	✗	✗
Rogerio et al. 2021 [34]	✗	✗	✓	✗	✗	✗
Miguel et al. 2009 [46]	✗	✗	✗	✓ sewl	✓	✗
Matheus et al. 2020 [31]	✗	✓ sm	✗	✗	✗	✗
Seiga et al. 2017 [28]	✗	✗	✓	✗	✗	✗
Sina et al. 2016 [19]	✗	✗	✓	✗	✗	✗
Sigitas et al. 2013 [40]	✗	✗	✗	✓	✗	✗

2.3 Data-Driven methods

This involves using machine learning techniques on large datasets to model and predict the behaviour of deformable objects. The models learn these behaviour from empirical data. This way of modelling is particularly used in scenarios where creating an accurate physical model is very challenging due to the complex unpredictable nature of the deformable objects.

2.3.1 Neural Networks

In [52], Wang et al used Action Prediction Network (APN) and a Configuration Prediction Network (CPN) to model the complex pattern interactions between rigid and soft body like DLO (Eg:- cables) for the transportation of rigid box using cables as shown in figure 2.8.

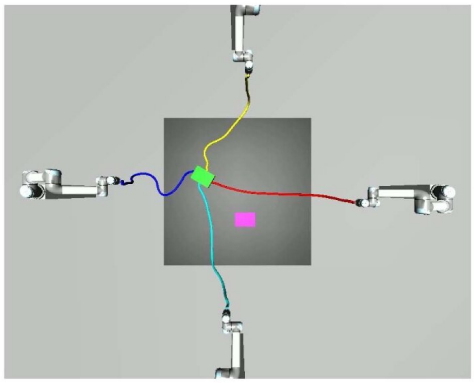

Figure 2.8: Rigid and Soft body interaction based on neural network model [52]

2.3.2 Learning based

In [56], Zhaole et al used a stationary dexterous hand to manipulate a cable for some goal conditions like grabbing, pulling, end-tip position control etc. Reinforcement learning was used to generate policies for the goals as shown in figure 2.9.

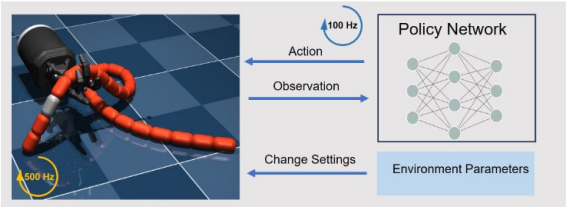

Figure 2.9: DLO ((cable) manipulation using a reinforcement learning based model [56]

2.4 Summary

The different methods of modelling were discussed above. The physics based method was able to capture the dynamics of the objects but it was computationally intensive for both lumped and distributed methods. The geometric methods were simple based on fewer dimensions and parameters but it does not give the dynamics and assumes quasi-static motions. The learning based methods are capable of capturing the model without knowing the exact analytical equations but it is very hard to get the model through this method as it requires a large data to train and setting up the initial infrastructure is very time consuming. Due to all these reasons, geometric method is preferred as the intended application does not require fast dynamic motion and quasi-static motion works for the target application. Further, in geometric methods catenary based modelling is preferred as it is a simplistic model with one parameter and also describes the shape of cables in all possible configurations.

3 Modelling

The modelling of quadrotors are well studied and established in literature. The modelling of a deformable object like collecting or cargo net is not well studied and non trivial. Hence, this section focuses more on modelling of the net. For the simplicity of modelling, the net will be modelled as multiple DLOs.

3.1 Net

A net is a grid like structure which blocks the passage of large solid items and allows passage of fluids and small items, depending on the size of the grids. It is flexible and light weight, made up of fiber (nylon, hemp etc) or other materials based on the intended task. For light load pickup tasks as intended in this project, hemp based nets are preferred as they are non-elastic / in-extensible and resistant to salt water.

In static equilibrium, the natural shape of a free hanging net held at it's corners is formed due to the effect of force balance between uniform gravitational field and tensions forces in the net. This is very similar to shape formation in a catenary (DLO). Hence, the net can also be modelled as a combination of DLOs. This minimalistic model helps to capture the natural shape, kinematics of a net.

3.2 Catenary curve

The catenary curve is obtained when a cable supported at both ends is freely suspended under it's own weight in the presence of uniform gravitational field. The catenary is a Deformable Linear Object (DLO) because it's length is bigger than other dimensions like width and thickness. The reason why it's called "linear" is because it is one-dimensional object, like a line or curve having a continuous shape and extending in a single direction (along it's length).

The catenary has a very long and interesting history. It started when mathematicians attempted to describe the shape of hanging chains and ropes. In 1638, Galileo incorrectly identified the shape as parabola [18]. Later in 1691 Johann Bernoulli, Leibniz, and Huygens independently derived the correct equation for the catenary, describing it with the hyperbolic cosine function. Due to this it's name is derived from latin word called 'catena' meaning chain. This curve is also called the alysoid and chainette. It is widely used in construction and analysis of structures like Bridges, Gateway Arch in St.Louis etc.

The mathematical intuition behind catenary is hard because it is described by hyperbolic cosine function which belongs to a group of functions called transcendal functions meaning it cannot be expressed as algebraic combinations of elementary functions. The mathematical intuition behind this class of curves are explained in detail in section 3.2.1.

The use of catenary cable in modelling nets simplifies the complexity of dealing with an infinite dimensional configuration space [15]. At the same time, it gives a minimalistic and accurate representation of the shape of the net based on it's natural dynamics (natural equilibrium position). Further, the catenary model has the capability to accurately describe both taut and very saggy cables with minimum degrees of freedom.

3.2.1 Equations of catenary curve

The equation of a catenary curve is central to understand it's properties and how to use it for the application in the project. It is expressed in cartesian co-ordinates as shown in equation 3.1 . The hyperbolic cosine term in the equation shows that it is an even function meaning the curve is symmetric about y axis (vertical axis) because the hyperbolic cosine is formed by the average of e^{x} and e^{-x} curves.

$$y = a * cosh(\frac{x - x_0}{a}) + b \tag{3.1}$$

the symbols in the equation are explained as

a is the radius of curvature of the catenary curve. It measures how sharply the curve bends.
x_0 is the x-coordinate of the symmetrical point of the catenary. It is the point where the catenary curve reaches it's minimum vertical position and is symmetric about this point.
b is the y-cordinate of the symmetrical point of the catenary or vertical offset of the catenary curve. It represents the distance by which the entire curve is shifted vertically from the origin.
x is any x-cordinate point between the end points of the catenary curve.

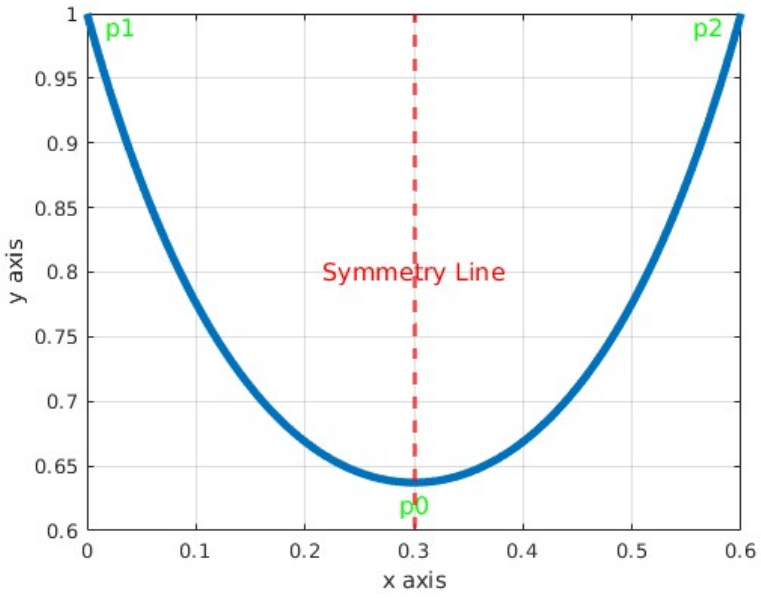

Figure 3.1: Catenary visualisation based on equation 3.1

The curve is represented in 2-dimension (2D) with x and y co-ordinates as shown in figure 3.1 . The curve is symmetric about the symmetry line and it is very similar to the figure 3.2 which shows the intuition behind the equation of the curve. In figure 3.1, the points p1 and p2 represent the end points or supporting points of the cable. The point p0 is the symmetry point.

The catenary curve is a static curve meaning, it does not accelerate and it is always in static equilibrium, the forces are balanced. Hence, the summation of forces in the cable is zero. It is a one parameter curve projected on a 2D plane. The parameter "a" called as radius of curvature, can also be called as catenary number or stretch of the cable. It determines the deformation of the cable or DLO. A detailed explanation of this parameter is written in 3.2.2.

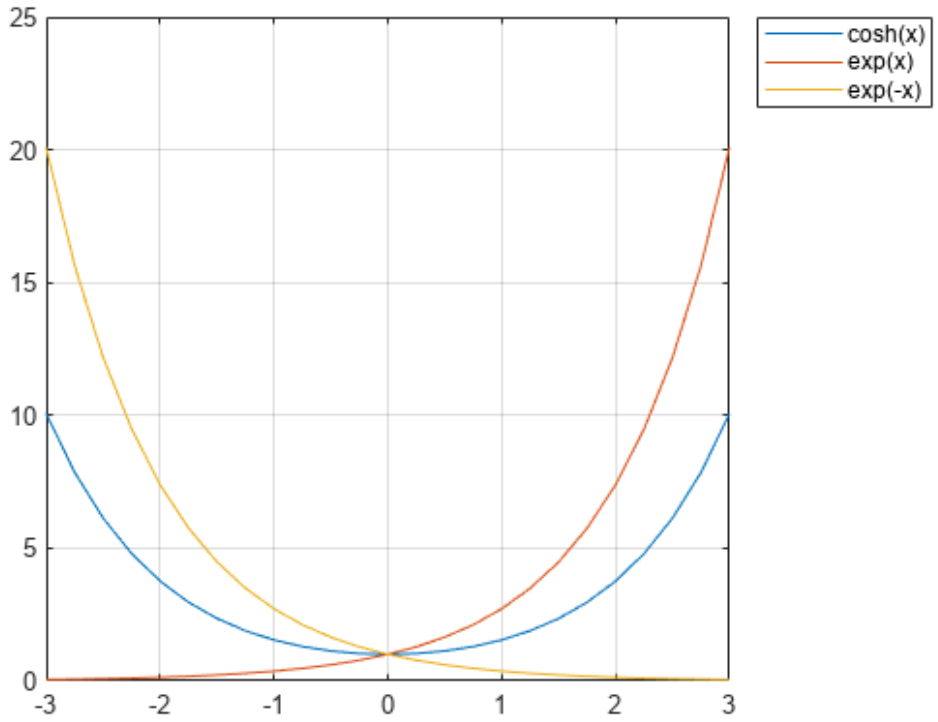

Figure 3.2: Catenary visualisation as avergae of positive and negative exponential functions [50]

3.2.2 Catenary Parameter

The parameter "a" of the catenary is called as catenary number. It controls the shape and size of the catenary curve. It depends on physical properties of the cable like weight per unit length, tension as shown in equation 3.2 . It can only have a positive value as it represents the pulling of a cable and having negative stretch or pushing of a cable has physically no meaning. Hence, it can be treated as a scaling factor and having a negative value will mean that the curve is flipped.

$$a = \frac{T_0 * L}{mg} \tag{3.2}$$

the symbols in the equation are explained as

a is the radius of curvature of the catenary curve. It measures how sharply the curve bends.
T_0 is the tension at the symmetry point of the cable.
L is the length of the cable.
m is the mass of the cable.
g is the gravitational field.

The problem is tension T_0 at x_0 or any point x cannot be calculated without knowing the catenary number (a). Hence, equation 3.2 cannot be used to find parameter (a). Inorder to find the parameter from the known position of end points of the cable p1 and p2 as shown in figure 3.1, the formula should be based on position instead of tension of the cable.

$$0 = -\frac{\sqrt{L^2 - v^2}}{2} + a * sinh(\frac{abs(x_1 - x_2)/2}{a}) \tag{3.3}$$

$$0 = -\frac{\sqrt{L^2 - v^2}}{2} + a * sinh(\frac{d/2}{a}) \tag{3.4}$$

the symbols in the equation are explained as

L is the length of the cable.
a is the catenary number
d is the absolute difference between the horizontal distance of the end points.
v is the absolute difference between the vertical distance of the end points.

The equation 3.4 represents the relationship of catenary parameter (a) and the position of end points of the cable. Finding it by this method is still hard as it does not have an analytical closed form solution. Hence, it can only be found by finiding the roots of the non-linear equation by using numerical methods.

These 2 methods are used to find the roots of non-linear equation in MATLAB.

Bisection Method

It is used to find the root of a continuous function $f(x)$ within a specified interval $[a,b]$, where the function changes sign. For example, $f(a) * f(b) < 0$

$$f : [a,b] \rightarrow \mathbb{R} \tag{3.5}$$
$$\text{i.e., } f(a) \cdot f(b) < 0 \tag{3.6}$$
$$C_n = \frac{a_n + b_n}{2}, \qquad \text{i.e., } a_n, b_n, C_n \in [a,b] \tag{3.7}$$
$$\left|f(C_n)\right| < \epsilon \tag{3.8}$$

The method runs until the condition in equation 3.8 is satisfied. This method is simple and has a slower convergence. The fzero matlab function has a similar functionality and it is used for the analysis.

True Region Method

In this method, the roots is found by linear interpolation of a secant line between end points. The linear approximation is repeated and a new endpoint is used to update the interval. This is done until the method converges to find a root than is less than the specified threshold.

$$f : [a,b] \rightarrow \mathbb{R} \tag{3.9}$$
$$\text{i.e., } f(a) \cdot f(b) < 0 \tag{3.10}$$
$$C_n = \frac{a_n \cdot f(b_n) - b_n \cdot f(a_n)}{f(b_n) - f(a_n)}, \qquad \text{i.e., } a_n, b_n, C_n \in [a,b] \tag{3.11}$$
$$\left|f(C_n)\right| < \epsilon \tag{3.12}$$

The method runs until the condition in equation 3.12 is satisfied. The True Region method is focused on global optimization over complex solution spaces. The fsolve matlab function has a similar functionality and it is used for the analysis.

Summary

The bisection method is the preferred method to find the roots because although it has a slower convergence compared to true region method, it is guaranteed to find a root. Another reason is for highly non-linear functions like the transcendal equations (eg:- hyperbolic cosine) the slope angle can be nearly zero in some cases. In these, situations true region method will struggle to find a solution and the bisection method will reliably find a solution. Due to these reasons, bisection method is chosen as the preferred method.

3.2.3 Other equations of a catenary curve

The other unknowns in equation 3.1, can be found by computing their computing their own equations given the required parameters needed for them are given. The horizontal and vertical co-ordinates of the symmetric point are calculated based on equations 3.13 and 3.14 respectively. The length of the curve at any particular point can be found using the equation 3.15 .

The horizontal co-ordinate of the symmetry point is

$$x_0 = \frac{x_1 + x_2}{2} - (sign(x_1 - x_2) * sign(z_1 - z_2) * (a * atanh(v/L))) \tag{3.13}$$

The vertical co-ordinate of the symmetry point is

$$b = z_1 - a * cosh(\frac{x_1 - x_0}{a}) \tag{3.14}$$

The length of curve

$$L = a * cosh(\frac{x - x_0}{a}) \tag{3.15}$$

The tension along the horizontal and the vertical axis can be analytically found using the equations 3.16 and 3.17 respectively.

$$T_h = mga \tag{3.16}$$

$$T_v = mgL \tag{3.17}$$

3.3 System Model

The net is modelled as 4 cables (DLOs) with one end of each cable attached to each quadrotors and other ends of the cables connected at a point, thereby connecting the whole system together. This system is represented as an image in figure 3.3. The 4 catenary model is a minimal and most accurate kinematic representation of an Aerial NET (ANET).

3.3.1 Modelling assumptions

These are the assumptions used in modelling the net -

- **Flexibility -** The cables are assumed to be flexible meaning that the cables are incapable of developing internal forces other than tension.
- **Inextensible -** The cables are assumed to not change in length throughout the operation.
- **Quasi-Static -** The cables are assumed to move at very slowly at a constant velocity such that the static equilibrium of cable shape is guaranteed.

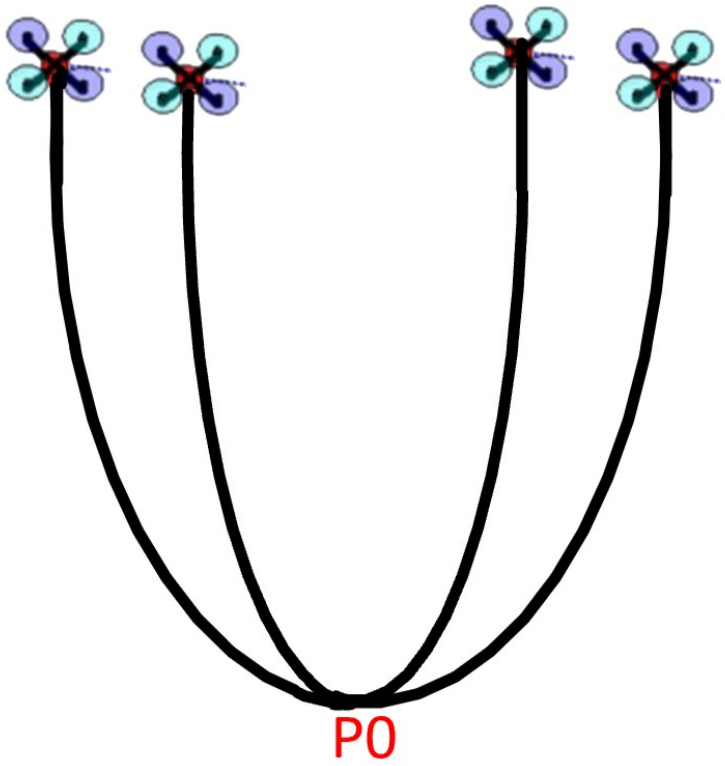

Figure 3.3: System model representing a physical net carried by 4 quadrotors, the net is modelled as 4 DLOs (cables)

3.3.2 Modelling hypothesis

There are 3 modelling hypothesis taken into account and all three of them are verified by experiments. The modelling assumptions are -

- **Case I -** Two flexible in-extensible cables placed in a diagonal configuration with one of their end points at the same height and the other end point connected together at one point forms 4 catenary curves.
- **Case II -** When the unconnected end points of the catenary cables are at different heights. They can be represented by 4 catenary curves.
- **Case III -** When the cables carry a small load. The shape is still represented by 4 catenary cables.

The modelling hypothesis is shown as a pictorial representation as shown in figure 3.4.

3.3.3 Difficulty in the model

Inorder to represent a catenary curve, it requires the position of 2 endpoints as explained in section 3.2.1. The free end of the cables are connected to the quadrotors, hence it is easy to retrieve that position information. The position of the point connecting all the cables is difficult to find as there is no actuation points like quadrotor and the model requires the position of this point to represent it.

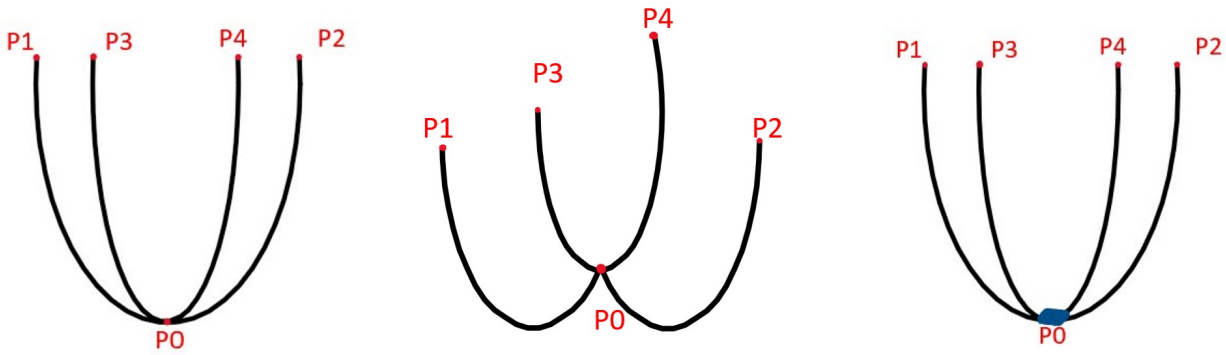

Figure 3.4: A pictorial representation of 3 cases of the modelling hypothesis

4 Experiments

This section describes the experiments and it's data analysis. The experiments are done to verify the modelling hypothesis as explained in 3.3.2.

4.1 Experimental Setup

The experiments are done indoor with the help of motion capture (MoCap) system to locate and localise the objects. It uses multiple IR cameras which tracks the reflective markers attached to the robot or the system. This helps to accurately localise them.

The system consists of a support structure and two long cables as shown in figure 4.1a. The cables are attached with reflective markers as shown in figure 4.1b . The reflective markers help in tracking the shape of the cables. There were some different kinds of loads as shown in figure 4.2 to test the modelling hypothesis and their weights are shown in table 4.1. The length of each cable is 1.76 meters. since the modelling hypothesis is around 4 catenary formation, each catenary will be around 0.88 meters or 88 centimeters.

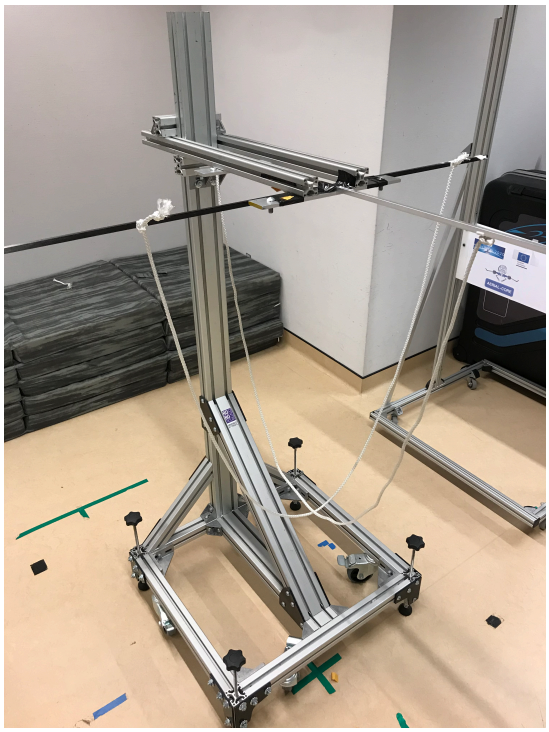

(a) Image showing the support structure with the cable before placing the reflective markers

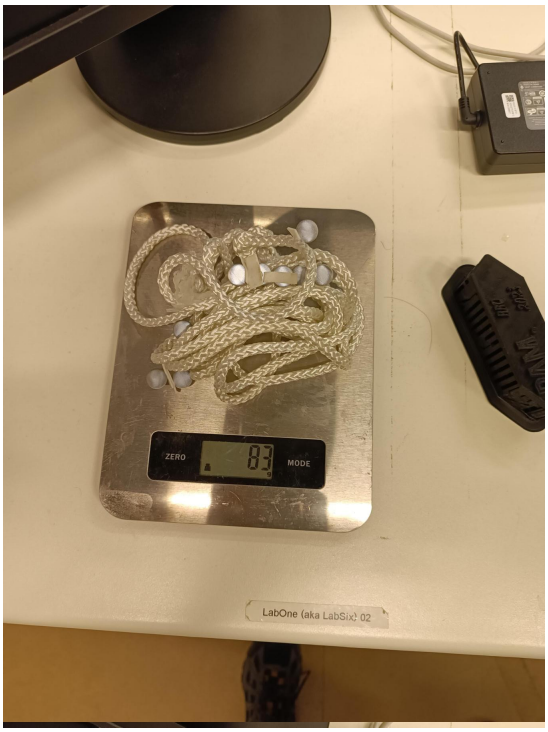

(b) Image showing the weight of the cable being tested, along with the reflective markers

Figure 4.1: Experimental setup

OBJECT	WEIGHT (grams)
Cables	83
Plastic sheat	7
Plastic cube	9
Plastic bottle	36

Table 4.1: Objects used in the experiment and their corresponding weights

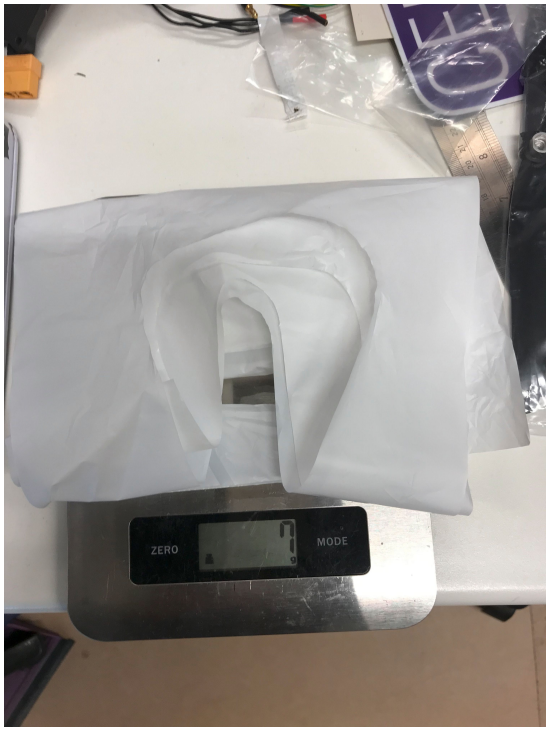

(a) Weight of a plastic sheat

(b) Weight of a plastic cube

(c) Weight of a plastic bottle

Figure 4.2: Weight of different loads used in the experiment

4.2 Data Collection

The data is collected for three different cases of modelling hypothesis. The problem with the data collection using the OptiTrack type of motion capture system is the data is not ordered or sequenced. Every time step has different sequence numbering for the data. This problem is overcome by using a post processing script in MATLAB, where the sequence number is corrected as the shape of the

cables are in a static configuration. The correction was done by numbering the data based on relative distance from a reference point in the system.

In the figure 4.3, it shows the system with cables freely hanging from the support. The top end of the cable attached to each support are at the same height. This configuration was used to collect the data and test whether these cables represent catenary cables.

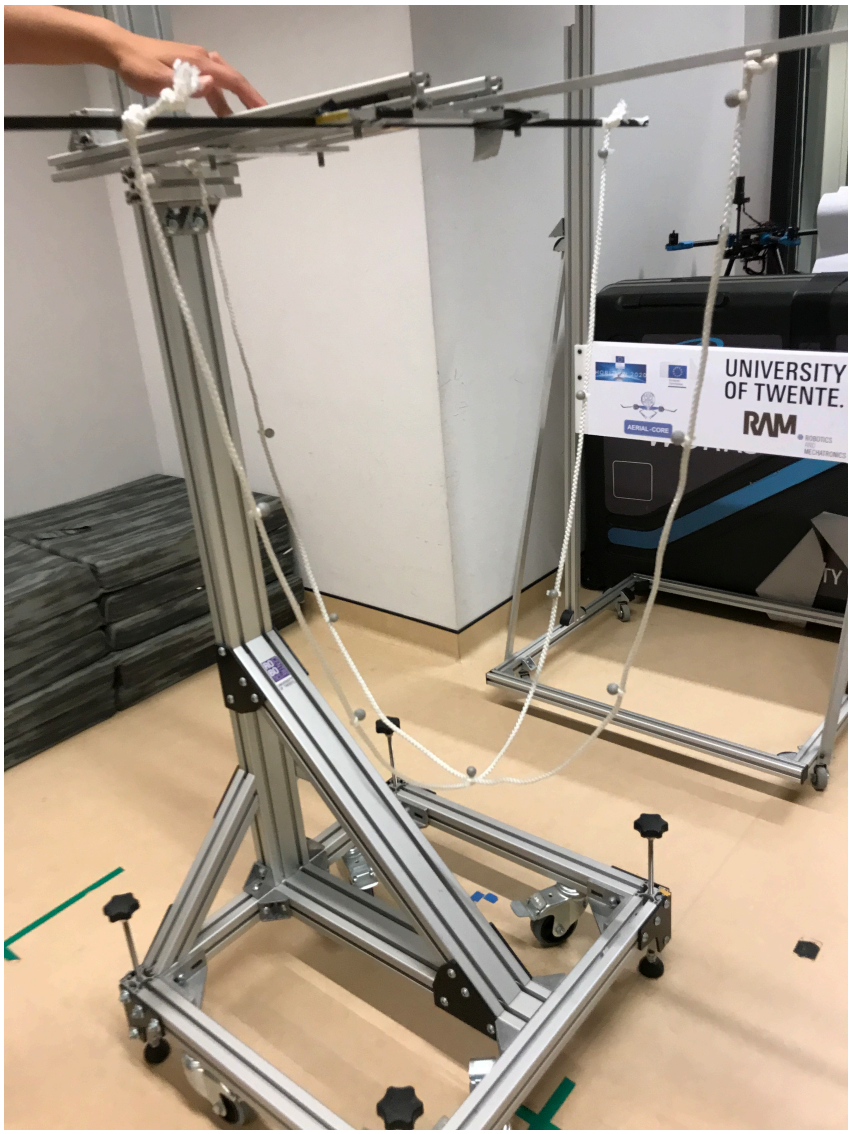

Figure 4.3: System configuration used for data collection in case 1 modelling hypothesis

The figure 4.4, it shows the system with cables freely hanging from the support similar to figure 4.3. This time the height of one of the cable is changed to be higher than the rest of the cables. This gives rise to a different shape. This system configuration was tested to see whether it represents a catenary cables.

The figure 4.5, it shows the system with cables freely hanging from the support similar to figure 4.3. In this configuration one of the ends of all the cables are attached at same height similar to figure 4.3, the only difference is the cables carry different kinds of loads ranging in their weight from lowest weight of a plastic sheat to the higher weight of a plastic bottle. These different configurations are

(a) Lateral view of the system

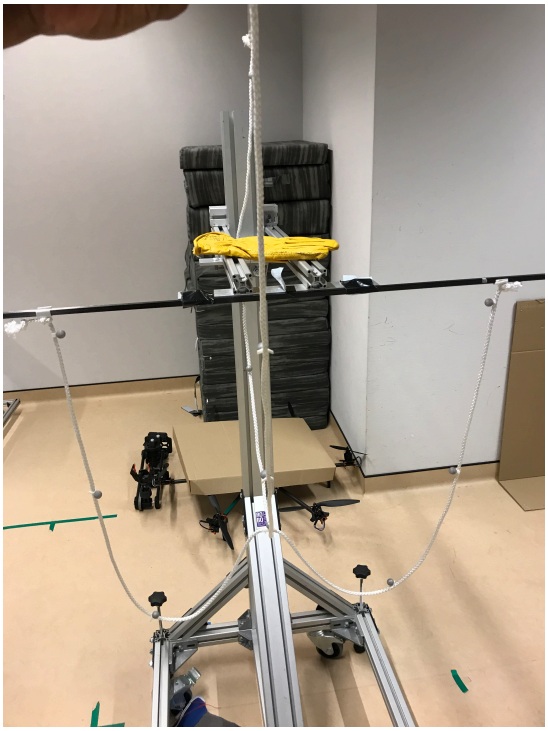

(b) Front view of the system

Figure 4.4: System configuration used in case 2 of modeling hypothesis

tested whether they still represent a catenary curves under different loading conditions of the cables.

4.3 Metrics

The metrics refers to a measurement method used to quantify, evaluate and track the performance of a system. In model verification, metrics assess a model's performance by comparing the accuracy of the theoretical predictions against real-world experimental data.

4.3.1 RMSE

Root Mean Squared Error (RMSE) is a regression type of model. It calculates the error between the observed data and the regression model. The catenary is used a regression model here and the observed data is the experimental data.

The RMSE is based on square root of Mean Squared Error (MSE), which is the average squared errors. It tells how well the data fits with the predicted error.

$$\text{RMSE} = \sqrt{\text{MSE}} = \sqrt{\frac{1}{n}\sum_{i=1}^{n}(Y_i - \hat{Y}_i)^2} \tag{4.1}$$

Where:

- Y_i represents the experimental values.
- $\hat{Y}_i$ represents the predicted value based on theoretical model.
- n is the number of data points.
- $\sum_{i=1}^{n}(Y_i - \hat{Y}_i)^2$ is the sum of the squared differences between actual and predicted values.

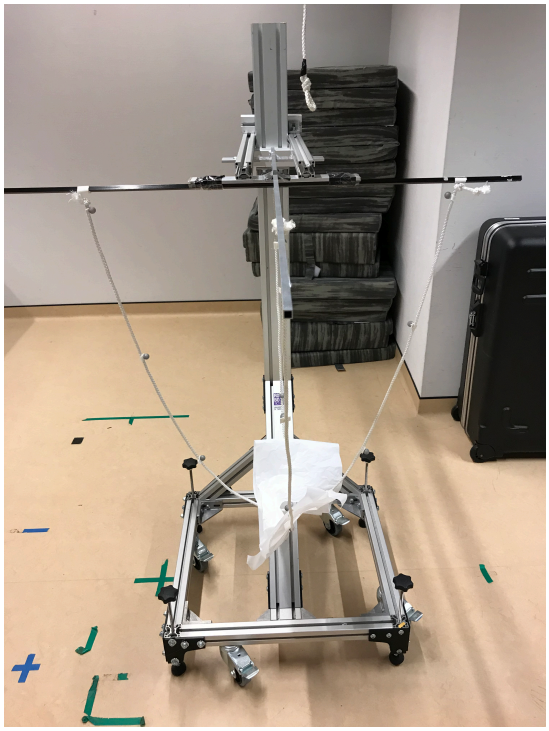

(a) cables at same height carrying a plastic sheat

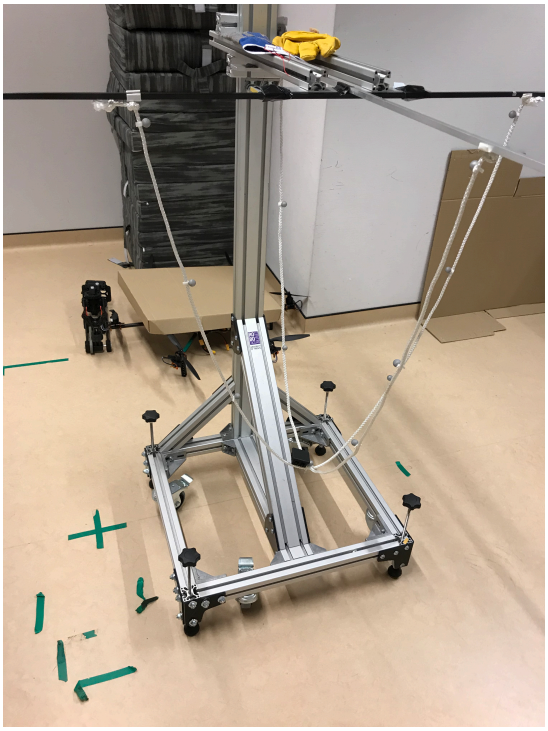

(b) cables at same height carrying a plastic cube

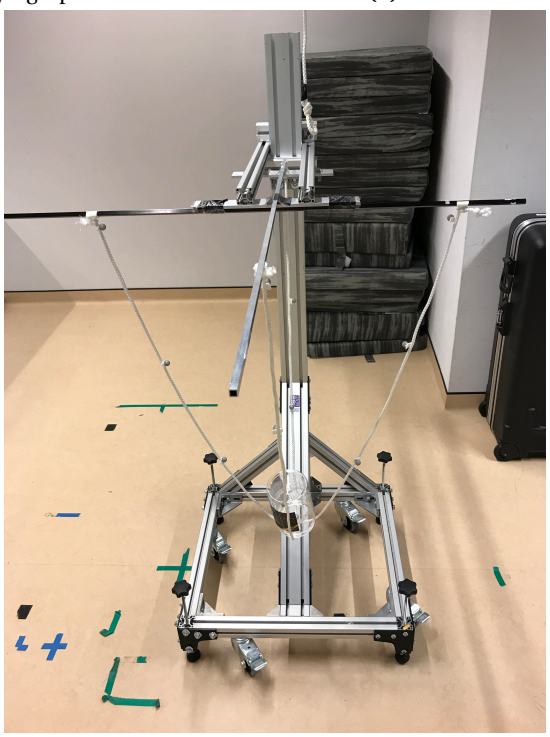

(c) cables at same height carrying a plastic bottle

Figure 4.5: System configuration used in case 3 modeling hypothesis

As the RMSE describes the error in prediction. The **lower the value of RMSE**, the **better the model**. If the RMSE value is **higher** then it is a **bad model** to represent the system.

4.3.2 R Squared (R^2)

The R squared (R^2) is another type of regression model, which explains the goodness of fit based on proportion of variance. The variance expresses how far the data points are compared to the mean

(average). It determining how well the model explains the variability in the data. The higher the variance the higher the degree of spread of data. Hence, the R squared uses the variance method to quantify the proportion of variance of the experimental data compared to the predicted model. Hence, the R squared metric is also called as co-efficient of determination.

This metric is different from the RMSE metric explained in section because the RMSE explains the absolute error and R square talks about the error from the mean (average). The Rquare formula is explained below in equation 4.2.

$$R^2 = 1 - \frac{SS_{res}}{SS_{tot}} \tag{4.2}$$

- SS_{res} (Residual Sum of Squares) is given by:

$$SS_{res} = \sum_{i=1}^{n} (Y_i - \hat{Y}_i)^2 \tag{4.3}$$

  - Y_i represents the real world experimental data for the i-th observation
  - $\hat{Y}_i$ represents the predicted value from the regression model or theoretical model.

- SS_{tot} (Total Sum of Squares) is given by:

$$SS_{tot} = \sum_{i=1}^{n} (Y_i - \bar{Y})^2 \tag{4.4}$$

  - Y_i represents the real world experimental data for the i-th observation
  - $\bar{Y}$ is the mean of the actual values in the predicted model.

In equation 4.2, The term $\frac{SS_{res}}{SS_{tot}}$ represents the proportion of the total variance that is not explained by the regression model. Since it is subtracted from 1 ($100 percent$), it explains the percentage of match between the experimental data and the actual model. An R^2 **value of** 1 indicates that the model explains 100% of the variance in the dependent variable **(perfect fit)**. An R^2 **value of** 0 indicates that the model is a **bad fit**. It explains none of the variance (the predictions are no better than using the mean of the dependent variable as a predictor). The values between 0 to 1 indicate the level of percentage of fit of the model with respect to the variance.

4.4 Verification of modelling hypothesis

The metrics explained in sections 4.3.1 and 4.3.2 are used to verify the modelling hypothesis.

4.4.1 Case I

The experimental data is collected for the system configuration as shown in figure 4.3. Then, the experimental data is plotted in a 3D graph, where the predicted model is also plotted to check the match between the models as shown in figure 4.6. The table 4.2 shows the metrics to evaluate the goodness of the fit. It can be seen that both RMSE and R^2 methods show a close fit with a very little error. In the case of RMSE, the value is close to zero almost at the scale of 10^{-2} showing a very close fit and in the case of R^2 it shows a fit close to 99.5% for all the 4 catenary curves. Hence, modelling hypothesis for case 1 is valid.

4.4.2 Case II

The experimental data is collected for the system configuration as shown in figure 4.4. Then, the experimental data is plotted in a 3D graph, where the predicted model is also plotted to check the match between the models as shown in figure 4.7. The table 4.3 shows the metrics to evaluate the

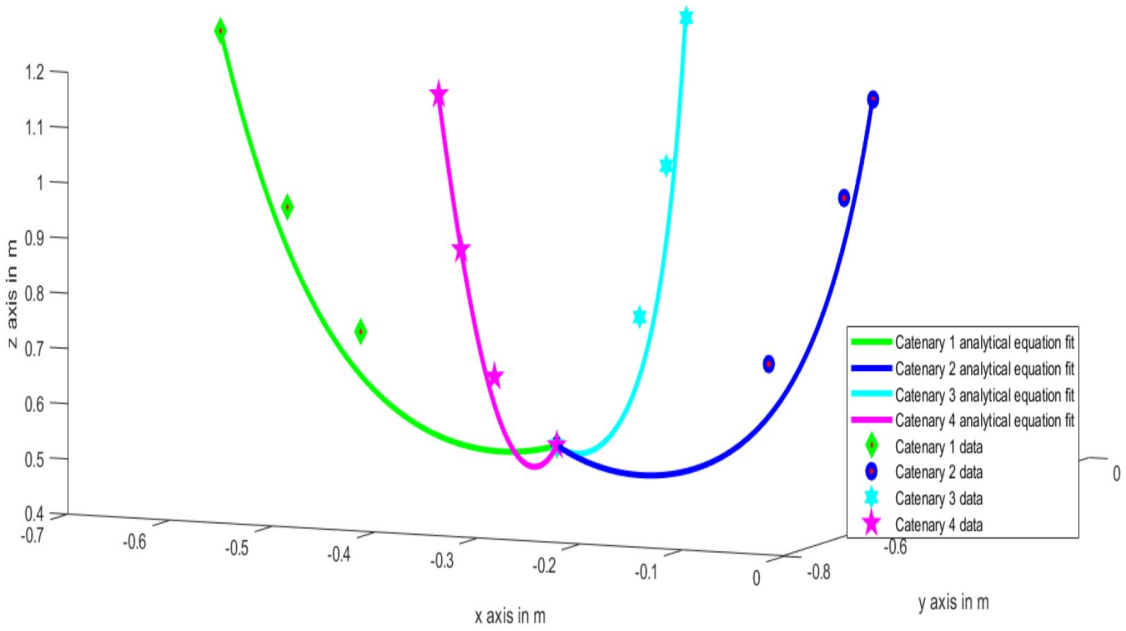

Figure 4.6: Plot used in the experimental data analysis of case 1 modelling hypothesis

Case-I	RMSE	R squared
Catenary 1	0.0335	0.9972
Catenary 2	0.0332	0.9967
Catenary 3	0.0404	0.9947
Catenary 4	0.0191	0.9991

Table 4.2: Metrics for case 1 of modelling hypothesis

goodness of the fit. It can be seen that both RMSE and R^2 methods show a close fit with a very little error even compared to case 1 in section 4.4.1. In the case of RMSE, the value is close to zero almost at the scale of 10^{-2} and 10^{-3}. This shows a very close fit and in the case of R^2 it shows a fit close to 99.8% for all the 4 catenary curves. Hence, modelling hypothesis for case 2 is validated.

Case-II	RMSE	R squared
Catenary 1	0.0587	0.9938
Catenary 2	0.0850	0.9848
Catenary 3	0.0024	1.0
Catenary 4	0.0012	1.0

Table 4.3: Metrics for case 2 of modelling hypothesis

4.4.3 Case III

This modelling hypothesis verifies static cables in a loaded condition. Three different loads are tested ranging from light to heavy load compared to the weight of the cable. The weights range from 8.4% , 10.8% and 43.3% for plastic sheat, plastic cube and plastic bottle respectively. The experimental data is collected for the system configuration as shown in figure 4.5. After that the experimental data is plotted in a 3D graph, where the predicted model is also plotted to check the match between the models as shown in figures 4.8, 4.10 and 4.10.

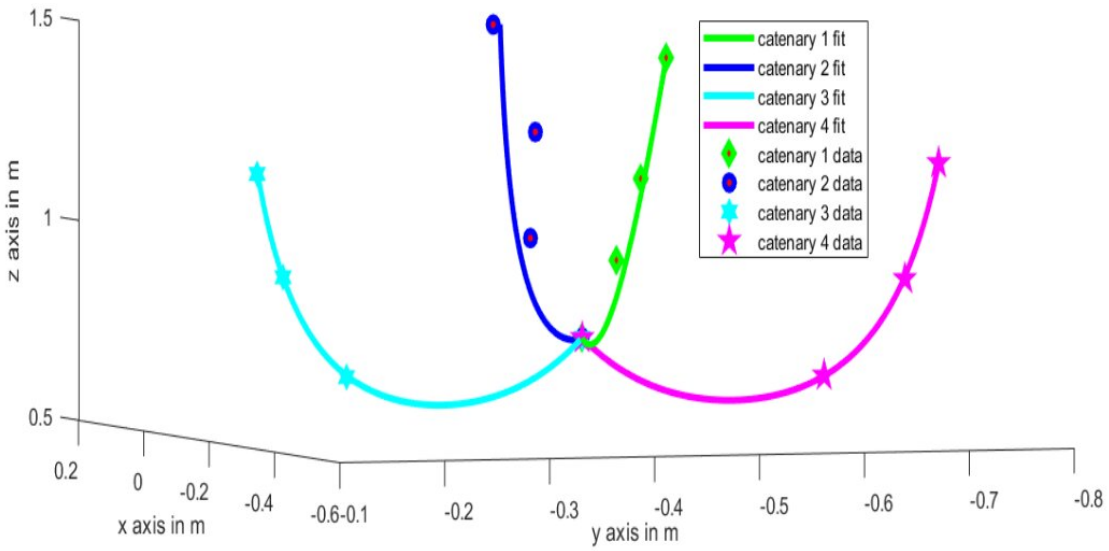

Figure 4.7: Plot used in data analysis of case 2 modelling hypothesis

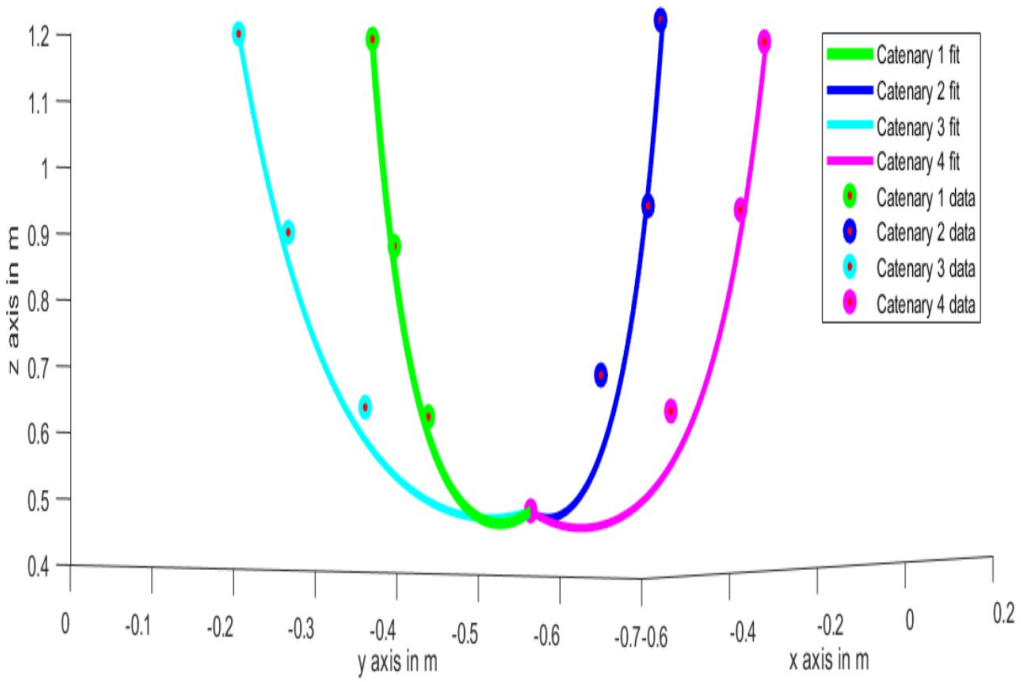

Figure 4.8: Plot used in data analysis of case 3 modelling hypothesis for plastic sheat load

The table 4.4 shows the metrics to evaluate the goodness of the fit. It can be seen that both RMSE and R^2 methods show a close fit. In the case of RMSE, the value is close to zero almost at the scale of 10^{-2}. It shows a very close fit and in the case of R^2 it shows a fit close to 99.6% and more for all the 4 catenary curves. Hence, modelling hypothesis for case 3 for a lighter load of around 8.4% could be said valid.

Case-III (plastic sheat)	RMSE	R squared
Catenary 1	0.0128	0.9995
Catenary 2	0.0328	0.9960
Catenary 3	0.0187	0.9986
Catenary 4	0.0277	0.9979

Table 4.4: Metrics for case 3 of modelling hypothesis with a plastic sheat as a load representing 8.4% of the total weight of the cables

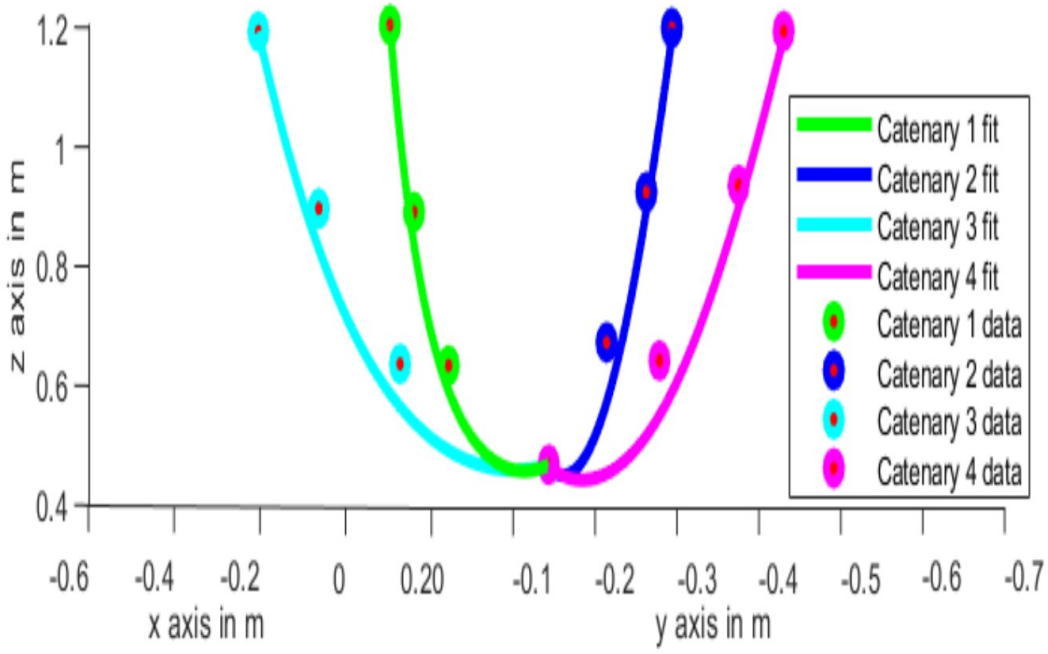

Figure 4.9: Plot used in data analysis of case 3 modelling hypothesis for plastic cube load

Case-III (plastic cube)	RMSE	R squared
Catenary 1	0.0174	0.9991
Catenary 2	0.0513	0.9903
Catenary 3	0.0326	0.9957
Catenary 4	0.0483	0.9935

Table 4.5: Metrics for case 3 of modelling hypothesis with a plastic cube as a load representing 10.8% of the total weight of the cables

The table 4.5 shows the metrics to evaluate the goodness of the fit. It can be seen that both RMSE and R^2 methods show a close fit. In the case of RMSE, the value is close to zero almost at the scale of 10^{-2}. It shows a very close fit and in the case of R^2 it shows a fit close to 99% and more for all the 4 catenary curves. Hence, modelling hypothesis for case 3 for a lighter load of around 10.8% could be said valid.

The table 4.6 shows the metrics to evaluate the goodness of the fit. It can be seen that both RMSE and R^2 methods show a close fit. In the case of RMSE, the value is close to zero almost at the scale of 10^{-2}. It shows a very close fit and in the case of R^2 it shows a fit close to 98.7% and more for all the 4 catenary curves. Hence, modelling hypothesis for case 3 for a lighter load of around 43.3% could be

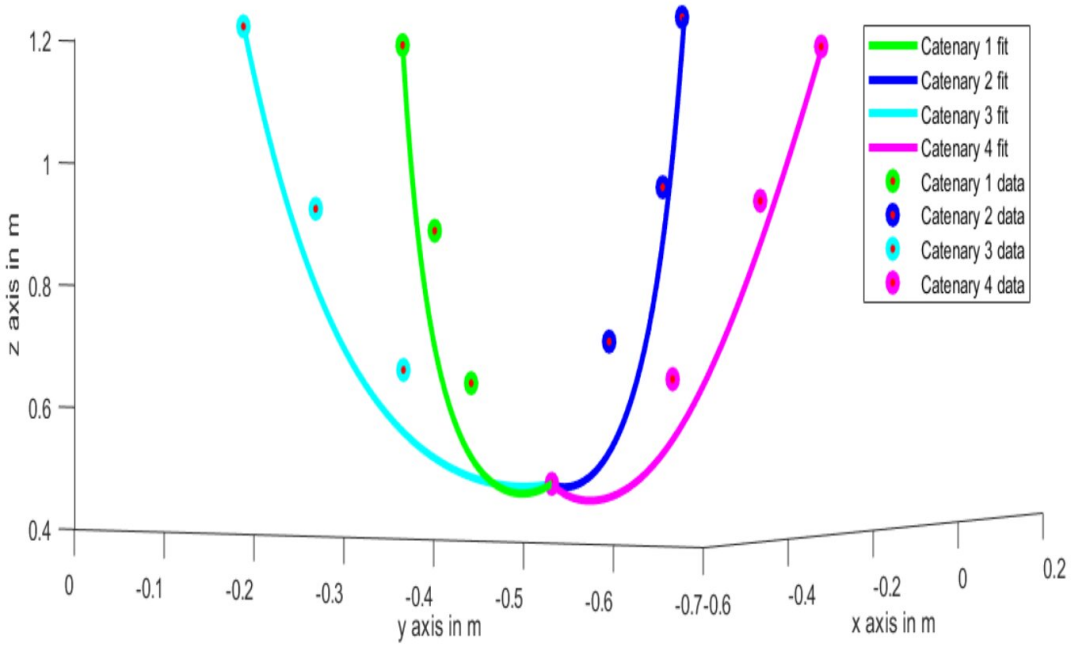

Figure 4.10: Plot used in data analysis of case 3 modelling hypothesis for plastic bottle load

Case-III (plastic bottle)	RMSE	R squared
Catenary 1	0.0579	0.9898
Catenary 2	0.0632	0.9855
Catenary 3	0.0475	0.9910
Catenary 4	0.0659	0.9878

Table 4.6: Metrics for case 3 of modelling hypothesis with a plastic bottle as a load representing 43.3% of the total weight of the cables

said valid.

4.5 Summary

The metrics in section 4.4 helped to validate all the three modeling hypothesis. This makes it possible to use catenary curve as a model for the system for all different kinds of configurations for both with and without load cases. The error of mismatch between the predicted model (theoretical model) and the actual experimental data is very less for all different configurations and loading conditions. The **overall goodness of fit** using **RMSE metric** was in the range of $\mathbf{10^{-2}}$ (very close to zero), exhibiting a very good fit. The overall goodness of fit using **R squared (R^2)** metric was in the range of **99%** (very close to 100%, exhibiting a good fit for variance based metric too. Hence , catenary based modelling satisfies all the three modeling hypothesis and suitable to model the system in all the different configurations of the net for both without and with load conditions (upto 43% weight of the cables).

5 Simulator

The developed system model needs to be tested in a simulation environment. The software framework that does this work is called as a simulator. The simulator does this by having a test model (second model) of the system which is generally more accurate than the first model and closer to real world based on the target application. This second model is used to test the system model developed in section 3.3. Hence, there are two models one is the system model used for development and other is a test model used by the simulator to simulate the system.

5.1 Sampling based energy optimisation

The catenary is a static curve due to this it will always attain a static equilibrium configuration. In this configuration, the forces in the cable are balanced. The forces being tension at the cable due to the support structure holding it's ends and the gravitational force acting along the entire length of the curve at every point of the cable. The static equilibrium attained due to force balance results in a stability. This static equilibrium can also be explained in terms of energy of the cable.

In equilibrium configuration the gravitational potential energy of the cable will be at local minimum [17]. Hence, this static equilibrium state of the cable can also be explained in terms of minimisation of potential energy between the two end points of the cable. This will represent the shape of the cable.

5.1.1 Main problem

Generally, if two points of a catenary cable are given it is easy to find all the other parameters of the cable a, x_0 and b respectively. In the case of the system model used in the project as shown in figure 5.1 (similar to figure 3.3 in section 3.3), one end of the cable is connected to the quadrotors and the other end of the cable is connected together. This point is called connecting point P_0 . The potential energy minimisatoon problem is done to find this connected point P_0 as there is no analytical expression to find it and without it other parameters of the catenary cannot be found.

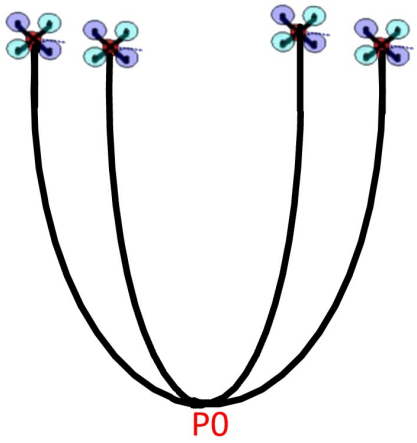

Figure 5.1: System model representing showing connection of all the 4 cables at the point p_0, forming other end of each cable

5.1.2 Principle of potential energy minimisation

The potential energy formulation of fiding the other end of the cable, point p_0 and ultimately the shape of all the cables in the system can be given by the equation 5.1.

$$J = \min_{p_0} \left(\sum_{i=1}^{n} \sum_{j=1}^{m} M_{ij} \cdot g \cdot y_{ij}(p_0) \right) \tag{5.1}$$

J is the potential energy for the entire cable.
p_0 is the point connecting all the cables.
n is the number of cables.
m is the number of individual points used to represent a cable.
M is the mass of each individual point in a cable,
g is the uniform gravitational field.
y is the height of the point from the ground. It is found using the equation 3.1 of a standard catenary.

The point p_0 is used to get other parameters of each cable like a, x_0 and b because these parameters require 2 points in a curve to find the depend variables like v (vertical distance between 2 end points), d (horizontal distance between 2 end points) as shown in equations 3.13 and 3.14

The minimisation of p_0 needs to satisfy the following condition in equation 5.2 . It means that the point p_0 is a real number and the distance between p_0 and other points supporting the cable should be greater than 0 and less than or equal to the total length of each cable

$$p_0 \in \mathbb{R} : 0 < \left| \bigvee_{i=1}^{n} p_i - p_0 \right| \leq L \tag{5.2}$$

n is the number of cables.
$\bigvee_{i=1}^{n} p_i$ is the logical OR operator, stating an OR operator between points p_1 to p_n
p_0 is the point connecting all the cables.
L is the length of each cable.

The sampling of points to find p_0 should definitely satisfy the condition of equation 5.2. There can be further optimisation inside this region to reduce the sampling and arrive at the shape faster.

The entire system consists of 4 catenary cables having one end of cables attached to each other and the other end of the cables placed in a support structure like a quadrotor as shown in section 3.3 and in figure 3.3. Inorder to test this method reliably and build it for the system in a modular way, first the method is tested for one single cable as shown in section 5.1.3 and then for the entire system as shown in section 5.1.4.

5.1.3 static configuration - one cable shape

Inorder to develop and test the energy optimisation method described in section 5.1.2. First one simple static configuration was chosen consisting of 2 cables connected at a point. The cables are assumed to be homogeneously distributed in mass and having equal length of 1 meters each. The connection point between the cables is p_0 and the other free end of the cables p_1 and p_2 respectively are kept at same height. Due to this the region of optimisation can be taken as a symmetry line along the symmetry line of the cable when treated as a single cable as shown in figure 3.1.

Inorder to verify the results of the energy optimisation, it was used to compare with analytical expression of a single catenary. Since the supporting points in this configuration is kept at same height, the two cables can be assumed to form a single catenary and this can be compared with the analytical

expression of a single catenary. For this, the position of the supporting points are held constant between all the iterations. The analytical expression of x_0 and b representing the horizontal and vertical components of the symmetry point will be the reference for co-ordinates of the point p_0 in 2-dimension (2D).

In figure 5.2, the energy optimisation method results in a shape of the cables by finding the connection point p_0 between the cables. The first cable is represented in red color and the second cable is represented in blue color. Around 100 samples were used to sample for the p_0 aling the symmetrical line, then for each sample catenary cables were drawn. After drawing the catenary cables for every sampled point, the cables are discretized into many points and each point is used to calculate the energy of the catenary cable based on equation 5.1. The sample point of p_0 which has the minimum potential energy is chosen as the right configuration.

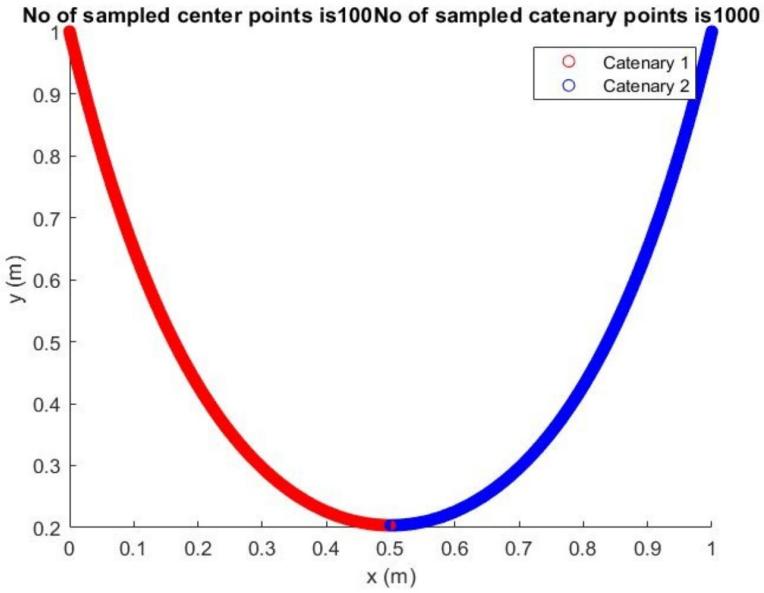

Figure 5.2: 2 Catenary cables formed based on energy optimisation between 2 cables shown as red and blue respectively

Since this method involves sampling and then discretization of the cables into points. The effect of sampling and discretization of the method is studied inorder to arrive at the right amount of samples and right amount of discretization. The main evaluation criteria used for this is the computation time and the position error of p_0 when compared to the actual value found out using analytical experession of a single cable reference. The p_1 is positioned at $(0, 1.0)$ and p2 is position at $(1.0, 1.0)$, this gives the position of p_0 at $(0.5, 0.2036)$. This was found using equations 3.13 and 3.14.

In figure 5.9, it shows the plots with details of each iteration of the sampling of $(p_0)$and discretization (n) effects. In figure 5.3, due to very less number of samples the shape is visibly not right as the number of samples is increaed in figure **??**, figure 5.14 and figure 5.6 the shape becomes more smoother and gives visible accuracy. It is seen that the discretization gives a better result in smoothness after keeping the number of samples constant. On increasing the number of samples and repreating the discretization effect as shown in figure 5.7 and 5.8 it is seen that is gives a even more sharper plots.

These results are closely analysed in the table 5.1, it can be seen that too few number of samples points for the connecting cable points (p_0) and discretization points (n) results in very large error

along z-axis. The number of samples for p_0 is increased to a consatnt values and the discretization is increased to get a good result around 100 and 100 respectively. Further, on increasing p_0 samples it results in increases the error in z axis unless the discretization of each cable (n) needs to be increased. This demonstrates the importance of (n) when compared to p_0 samples. Further, increased increasing p_0 samples requires the discretization (n) to increase significantly. This results in a very high computation time as shown in the last row of the table. Due to these tradeoff between p_0 samples and discretization (n) the number is chosen at 100 and 100 respectively.

Sampled Cable Connection Points (p_0)	**Discretization Catenary Points (n)**	**Computation Time (sec)**	**Error in Z Axis (cm)**
10	10	2.5	+3
100	10	7	-2.59
100	50	19	-0.84 (1)
100	100	40	-0.04
200	100	70	-0.43
200	500	310	0

Table 5.1: Table showing sampled cable connection points, sampled catenary points (p_0), computation time (n), and error in z axis.

5.1.4 static configuration - entire system shape

The shape of the entire system of cables, consisting of 4 cables was easily found by scaling up the energy optimization for 4 cables. Since the system is written in a modular way, this way of scaling up was made possible. A detailed explanation of the complete model and it's scaling up for shape and motion is explained in section 5.1.5 .

5.1.5 Motion of the system

The section 5.1.3 and 5.1.4 explained finding the shape of the cables in static configuration. Inorder to simulate the system, the shape has to be found when the system is moving. For this the shape finding needs to happen when the support points and the cable is moving. The good thing is this method still holds when the system is moving as the system is assumed to move in a quasi-static way.

Inorder to accomplish this the optimization needs to be run at every time step of motion by assuming every motion as a slice of static configuration because quasi-staticity assumes constant velocity. This also means that the region of optimisation needs to be increased in order to accommodate the motion.

motion of one cable

Inorder to develop and test the system in a modular way, first the motion of one cable is tested and then it is scaled for the entire system. The section 5.1.3 refers to finding the shape of the catenary cable in a static equilibrium configuration, now when the system moves the sampling region to find the cable connection point p_0 is increased based on the velocity of motion of the system. Hence, the sampling region of p_0 is not anymore a point, it is a cube. The width of the cube is based on the velocity of motion of the system.

In the figure 5.10, the catenary cable shape is formed based on the cube region of sampling for finding the connecting point p_0 between the cables. The potential energy cost of every point in the

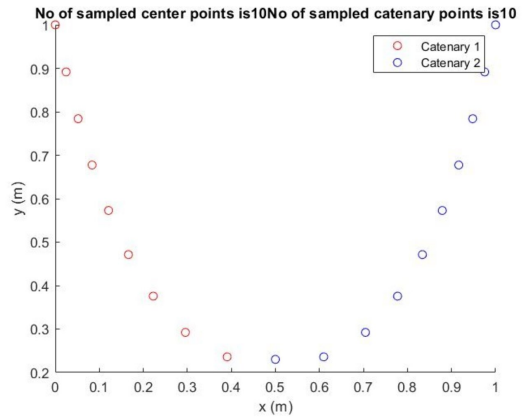

Figure 5.3: Catenary shape formation for 10(p_0) samples and 10 discretization (n) for each cable

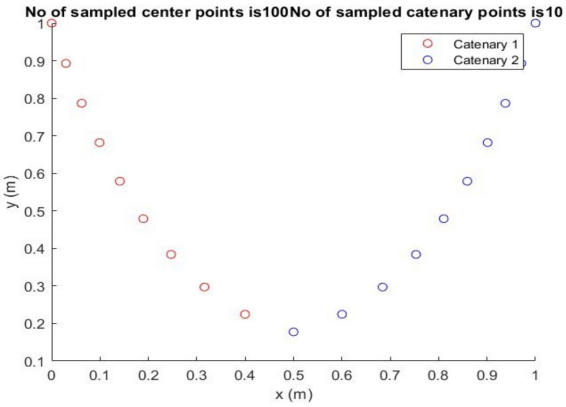

Figure 5.4: Catenary shape formation for 100(p_0) samples and 10 discretization (n) for each cable

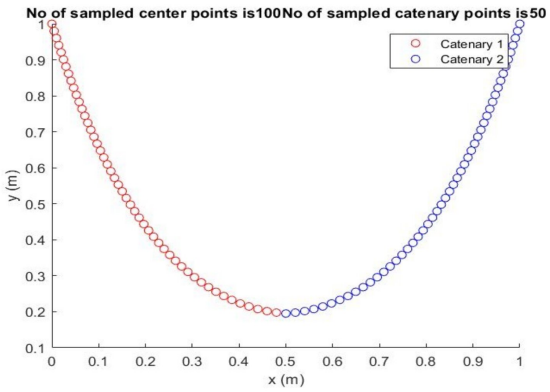

Figure 5.5: Catenary shape formation for 100(p_0) samples and 50 discretization (n) for each cable

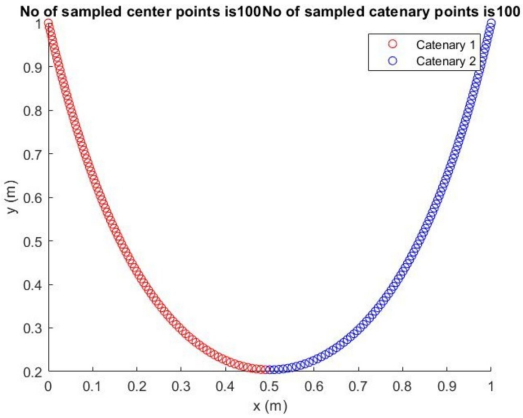

Figure 5.6: Catenary shape formation for 100(p_0) samples and 100 discretization (n) for each cable

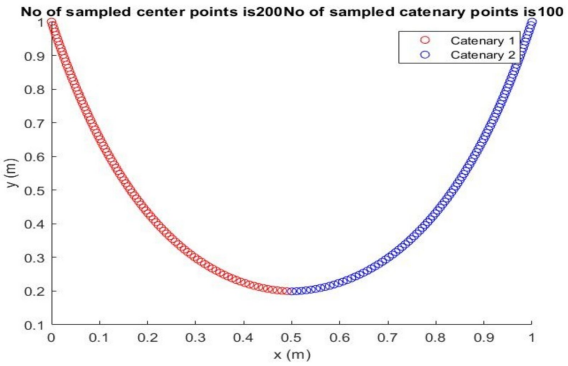

Figure 5.7: Catenary shape formation for 200(p_0) samples and 100 discretization (n) for each cable

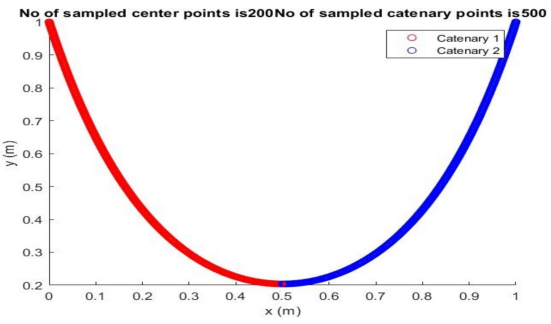

Figure 5.8: Catenary shape formation for 200(p_0) samples and 500 discretization (n) for each cable

Figure 5.9: The image shows different number of samples for (p_0) and different discretization (n) for each cable based on potential energy optimisation method

cable is shown in figure 5.11 and the point with the minimum cost is chosen to be the point for p_0 .

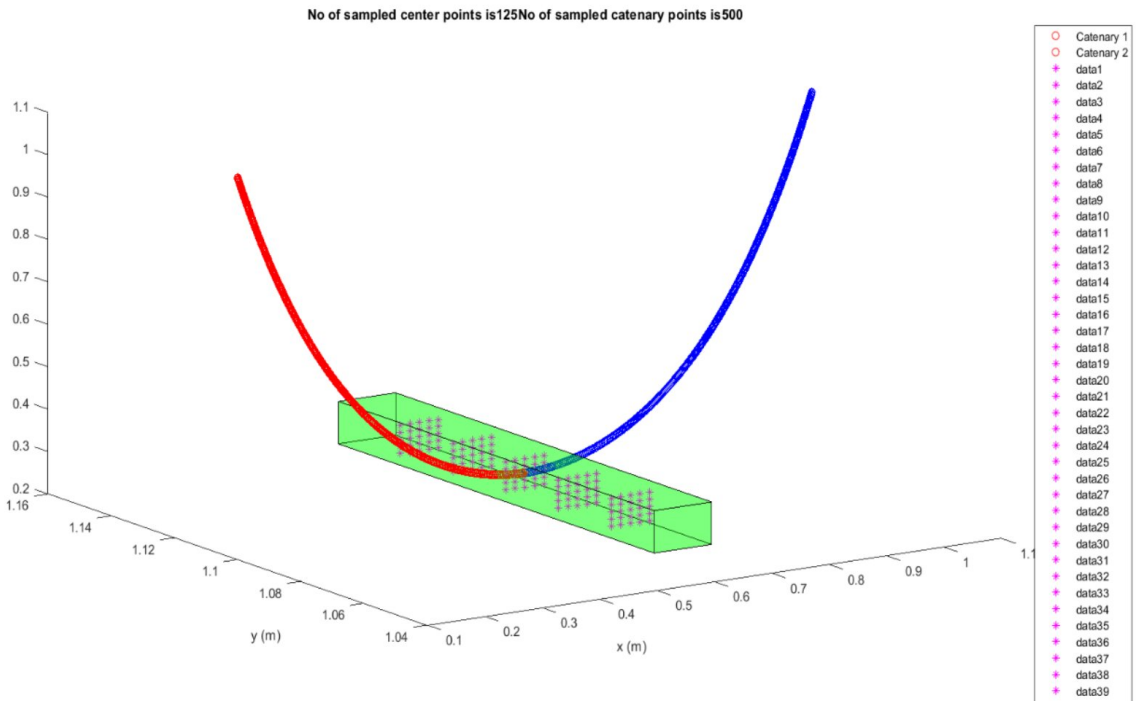

Figure 5.10: The image shows the shape of a catenary cable with cube region of sampling to find the connecting point p_0 of cables

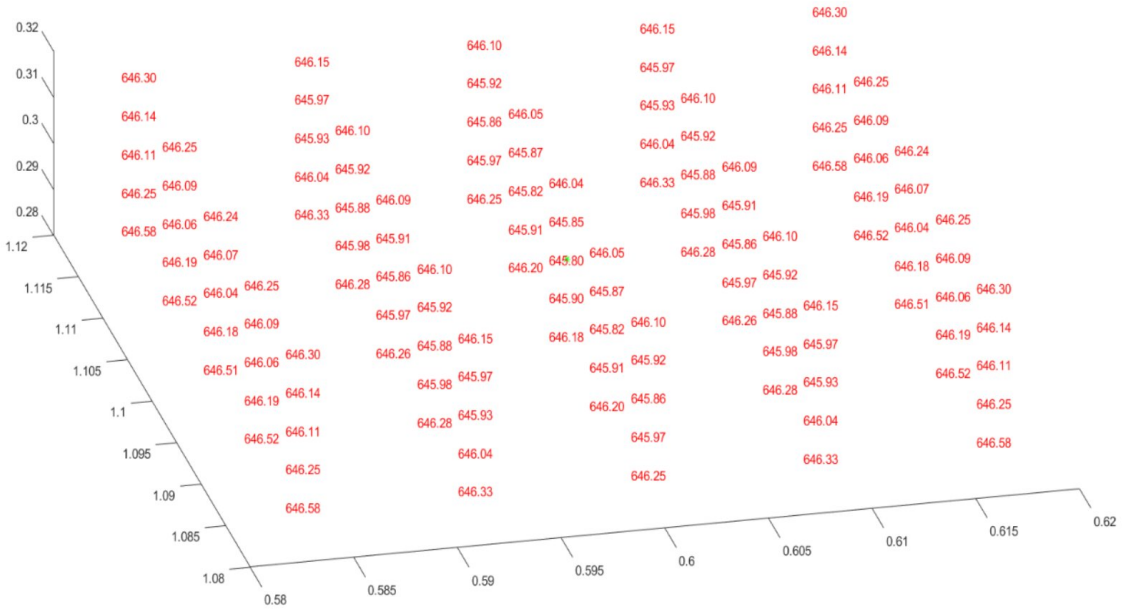

Figure 5.11: The image shows the value of potential energy of the entire system for every sampled point in the cube. It's performed to find the real cable connection point p_0

Currently, this method involves sampling the points in 3-dimensional (3D) space. Hence, the effect of sampling also depends on the closeness of sampling between the sampled points. Inorder to study the effect of closeness of sampled points and to arrive at a desired sampling number in 3D, a test similar to table 5.1 is performed as shown in figure 5.15 .

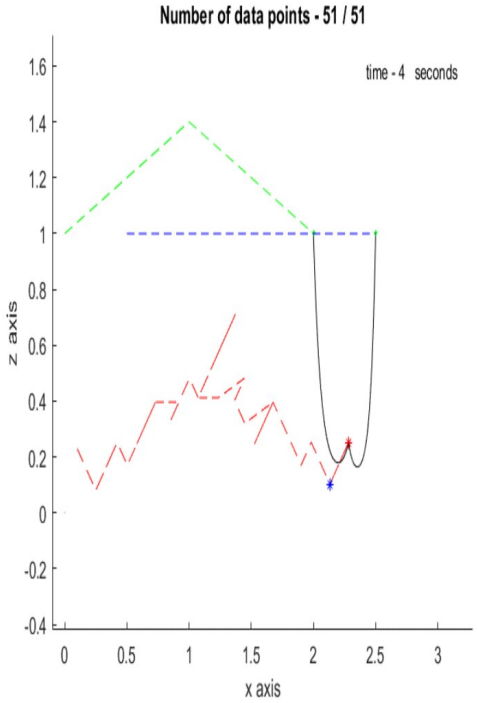

Figure 5.12: The result of motion of the cable with a 0.1 meter distance of samples inside the cube region of sampling for the cable connection point p_0. The motion of p_1, p_2 and p_0 are shown by green , blue and red respectively.

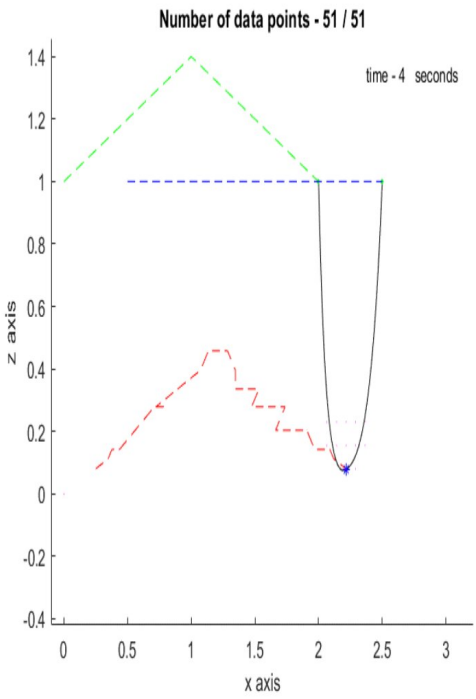

Figure 5.13: The result of motion of the cable with a 0.05 meter distance of samples inside the cube region of sampling for the cable connection point p_0. The motion of p_1, p_2 and p_0 are shown by green , blue and red respectively.

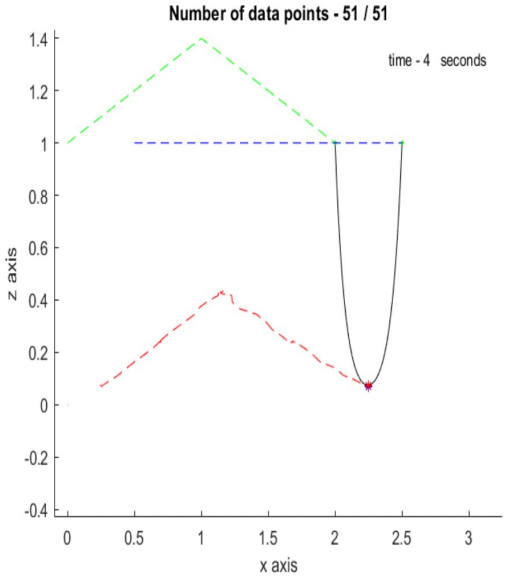

Figure 5.14: The result of motion of the cable with a 0.01 meter distance of samples inside the cube region of sampling for the cable connection point p_0. The motion of p_1, p_2 and p_0 are shown by green , blue and red respectively.

Figure 5.15: The plots show the effect of sampling distance inside the cube affecting the shape prediction of the cables (2 cables connected at p_0 point) during the motion of the cables caused by the attachment points p_1 and p_2.

The figure 5.15 shows that sparse sampling inside the cube region results in wrong shape calculation. Atleast $0.01 meters (1cm)$ of distance is required for sampling inside the cube to find the point p_0.

The figure 5.16 shows the motion of the cable along with the sample points in a cube. The distance between the samples inside the cube is chosen to be $0.01 meters (1cm)$ and also it can be seen that the cube region is not entirely filled with sample points because the cube width id formed based on the velocity of the system, this search region was further optimised by eliminating the sample points that exceeds the length of the cables as per the condition in equation 5.2. Although by doing this optimisation the **time taken to run this 4 second trajectory** is close to **14.5 minutes**, which is very high for a simulation of a **cable moving at 0.2 m/s**.

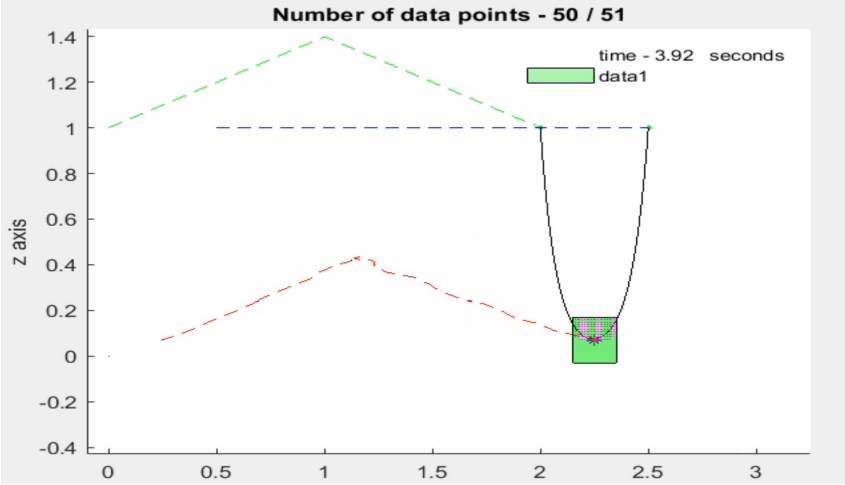

Figure 5.16: Image shows the motion of 2 cables connected at a point p_0 which is found by having a cube region of optimisation and the sampled points inside the cube is further reduced by following the length constraint of the cables.

motion of entire system

The model is scaled up for 4 catenary cables from 2 catenary cables. The figure 5.17 shows the motion of 4 cables.

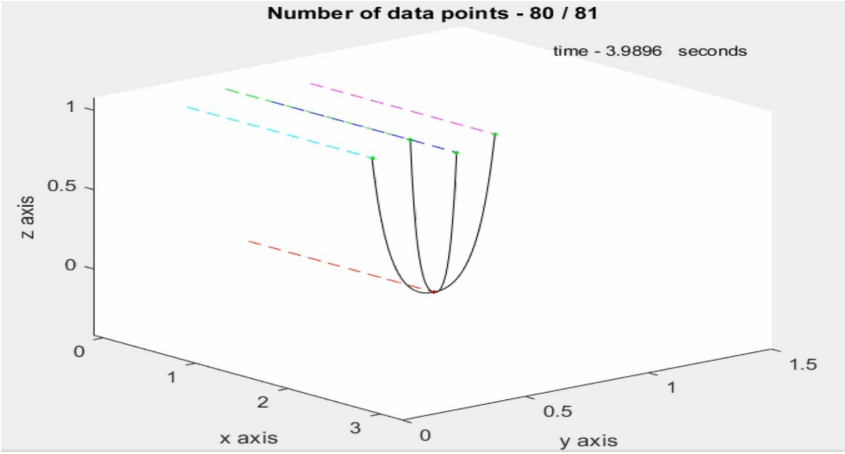

Figure 5.17: Motion of the complete system

Both a line region of optimisation based on symmetrical line and a cube based region of optimisation is tried. The symmetrical line region of optimisation is shown in figure 5.17 and it is used only for a

certain restricted type of motion. In the cube region of optimisation, the total **time taken to run a cube-based** region of optimization is **more than 30 minutes** for a **4 second trajectory**. This is very high simulation time and The image of it is not shown here. This is infeasible to be used as a test model to simulate the system.

5.2 Elasto-flexible simulator

This model consists of lumped masses interconnected by linear springs through passive spherical joints. This creates a flexible cable with extensible length which depends on the elasticity of the cable. The figure 5.18 shows the base model with 6 masses and 5 linear springs. As it can be seen the cable is not present in one plane this is due to the lumped nature of the cable masses connected by linear springs.

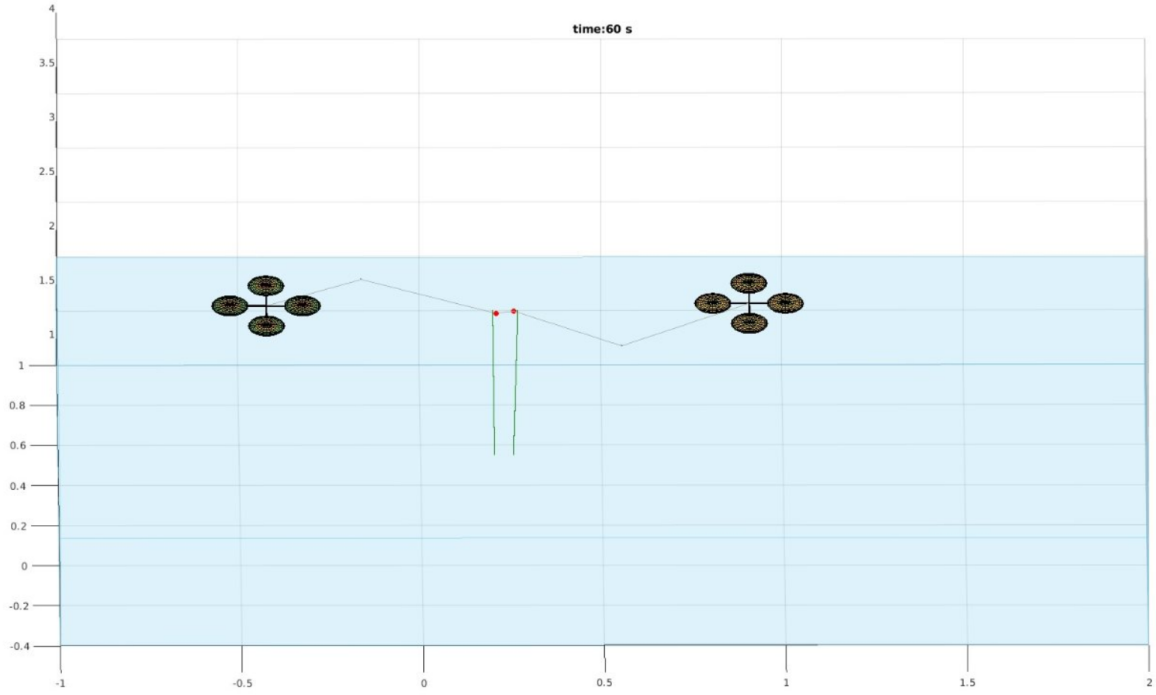

Figure 5.18: Elasto-flexible cable model, made of 6 masses and 5 springs

Inorder to overcome the problem and make the cable stay in the same plane as well as attain a continuous shape, the discretization of the cable is done. The figure 5.19a depicts a sparse discretization with 10 cm intervals per lumped mass for a 1 meter cable, while figure 5.19b illustrates a finer discretization with 5 cm intervals per lumped mass for the same cable length. It can be observed in both figures that as the discretization becomes finer, the cable appears closer to a continuous shape. Therefore, based on empirical analysis, a discretization of **5 cm intervals per mass is chosen**.

In figure 5.20, the elasto-flexible model is compared with the catenary model. It was observed that the length of the elasto-flexible model is 1.1 m for a 1 m cable. This discrepancy is due to the nature of the model being elastic, which caused a 10% error, equivalent to 10 cm. Since the error is significant, it is challenging to simulate and test these models for a fixed-length cable.

Inorder to reduce the error in shape the stiffness of the springs were increased but unfortunately it started making the model unstable. The possible reason could be not wnough damping as the damping in the model comes from the environment. Another addition to this is done by adding parallel dampers to the springs but unfortunately that also caused instability to the model during

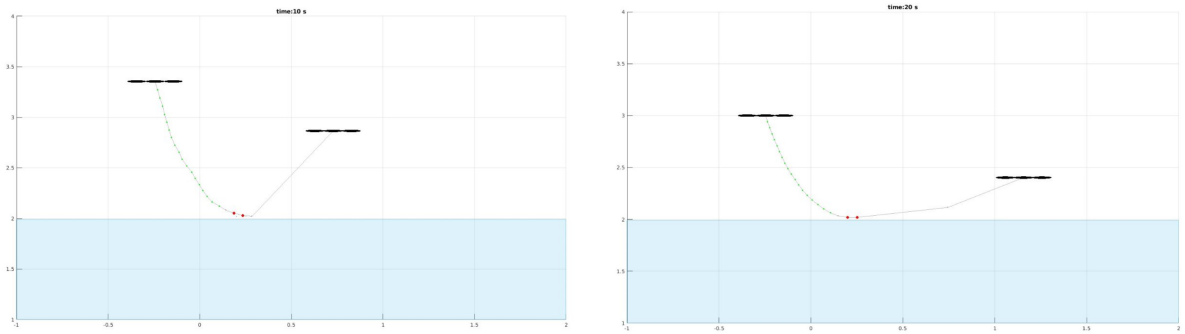

(a) Sparse discretization of one side of the cable

(b) Fine discretization of one side of the cable

Figure 5.19: Image showing different levels of discretization at one side of the cable for comparison

operation. This also showed that the tuning of the parameters cannot be done arbitrarily and the stability of the model is not reliable even after going through a lot of empirical tuning. This problem combined with the higher error in extensibility of the model made it not a viable model to be used for simulation for this project.

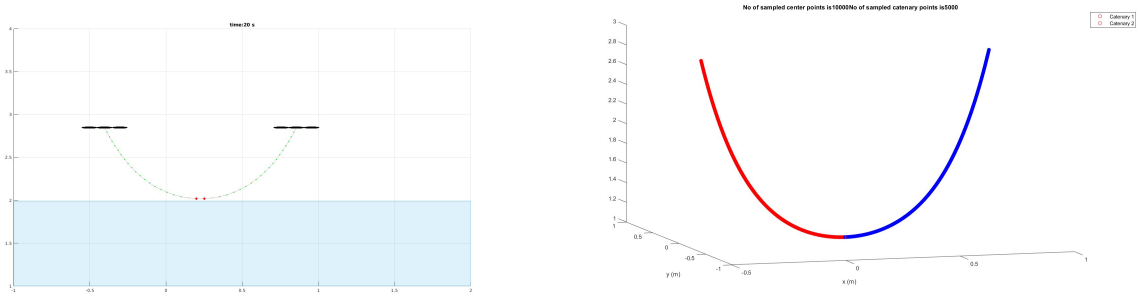

(a) Cable discretization of 5 cm per lumped mass is chosen

(b) Analysis of comparison of shape and length of the cable with analytical catebnary expression

Figure 5.20: The image shows the cable with finer discretization of 5 cm per lumped mass and analysing the shape and length of the cable

5.3 Physics based simulator

The physics based simulator model is faster, dynamic and more closer to reality. The newer gazebo based physics engine (Ignition Fortress) is used because the older gazebo classic was not smoother to actuate and control the model as it requires additional software (Plugins) to be written to control them, while the newer ignition engine has standard plugins meaning the actuation and controls are well tested and integrated for usage with minimal effort. Additionally, the newer ignition engine was faster and smoother. Due to this, the newer ignition gazebo is used for this method.

The main requirement while choosing the physics simulator was having capability to show the physics of multi-rotors, flexible cables and controlling them using Matlab/Simulink. These requirements were met by Ignition Gazebo engine, although interfacing with Matlab/Simulink was tough compared to Gazebo 11 (Gazebo classic). This problem was overcome by havig a ROS2 bridge between them.

5.3.1 Cable modeling

Since ignition gazebo is used for multi-rigid body simulations. The cable needs to be modeled as multiple rigid bodies in order for it to exhibit flexibility. Each rigid body in the cable is called as links and multiple links are connected by joints. The selection of joints is important as it decides how the cable behaves, it's degrees of freedom and flexibility. Generally, ball joint is best for this use case as it provides 3 degree of freedom (DoF) for rotation. Since ball joint is not yet present in ignition gazebo, this problem was overcome by using a combination two types of joints very close to each other to mimic a 3 DoF rotaion. The two types pf joints used where one revolute joint having 2 DoF rotation and other revolute join with 1 DoF ortaion placed as a small link of size 5 millimeters with the main link of 5 centimeters.

The cylindrical links was used to model the cable. The same level of discretization used in section 5.2 is used here. It can be seen from figure 5.21 that the cable forms a continuous and smooth shape when carried by the quadrotors. The connection point between the two cables is the green joint which represents the p_0 connection point.

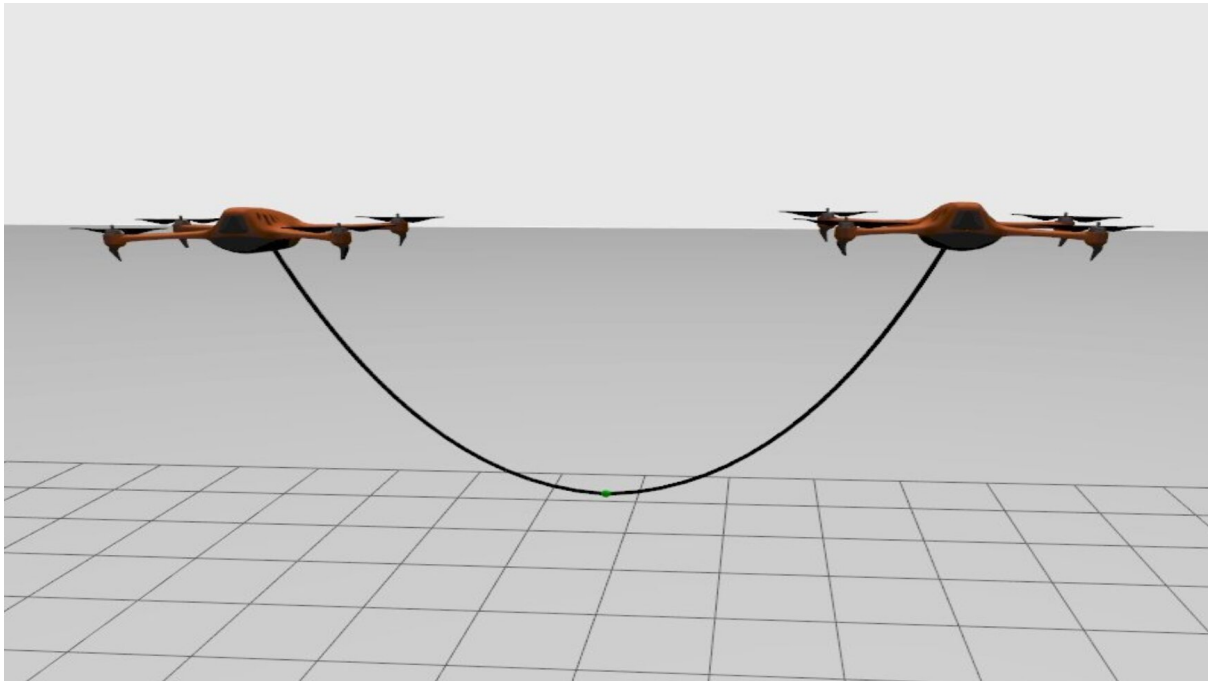

Figure 5.21: Inextensible flexible cable carried by 2 quadrotors

Further, the physical properties of the cable can also be set starting from mass of the links, moment of inertia, stiffness and damping of the joints can be set.

The total weight of the cables is kept at 200 grams as that is close to the weight of the nets in the physical world. The mass of the links is calculated based on this. Since each cable is 1 meter long and based on the level of discretization, there are 20 links and each link will have a weight of 5 grams as each individual entire cable will have 100 grams weight. The stiffness and damping of the joints were tuned empirically. Then, the moment of inertia is calculated based on equation 5.3

$$I = \begin{bmatrix} \frac{1}{12}m(3r^2+h^2) & 0 & 0 \\ 0 & \frac{1}{12}m(3r^2+h^2) & 0 \\ 0 & 0 & \frac{1}{2}mr^2 \end{bmatrix} \tag{5.3}$$

Where:

- I: Moment of inertia tensor
- m: Mass of each cylindrical link
- r: Radius of each cylindrical link
- h: Height of each cylindrical link

There are 2 major types of modelling format Unified Robotic Description Format (URDF) and Simulation Description Format (SDF). Inorder to make the models modular and avoid repetition of code blocks. URDF has a MACRO called XACRO and SDF does a similar thing with Embedded Ruby (ERB) text generator. The SDF with ERB was used to modularly change parameters and generate model of the cable.

In figure 5.22, the data of the links of the cable in gazebo is plotted in matlab, this is done by transferring teh data from ignition to matlab over the ROS2 bridge. The analysis showed a close fit with the catenary model. This was expected as the model was inextensible and had better discretization for the links.

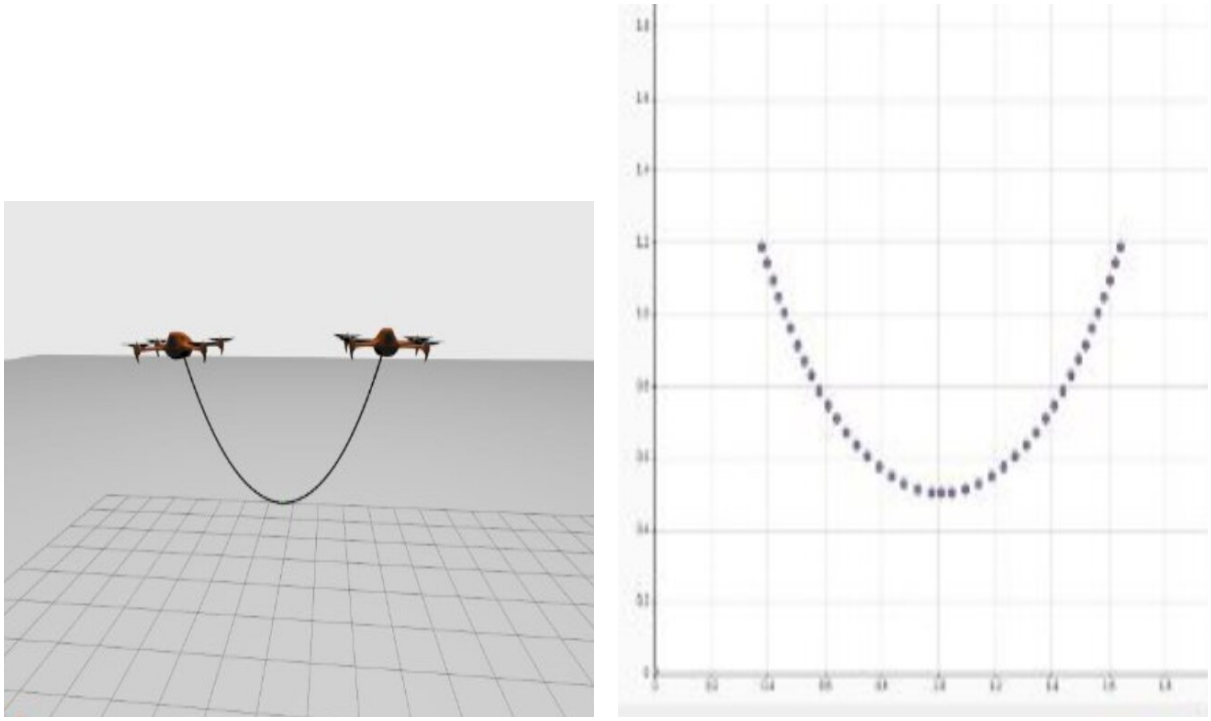

(a) Image of the cable in ignition gazebo and the position data of the links is sent to matlab for analysis

(b) Matlab plot of the link data used for analysis with analytical catenary model

Figure 5.22: Image showing the comparison cable model in ignition gazebo and the postion data of the same cable as a Matlab plot

In figure 5.23, it shows the cable being used as a platform for the development of control algorithms. It shows the shape manipulation of shape of a single cable in figure 5.23a and in figure 5.23b it shows the entire system having the possibility to do pose and shape manipulation of the cables using multiple multi-rotors.

5.3.2 Complete framework

The figure 5.24 explains the framework as a block diagram. The model of the system model (catenary based model) and the high level control algorithm are inside the Matlab/Simulink block and the simulation happens in Ignition/Gazebo, essentially doing co-simulation. This is made possible by using

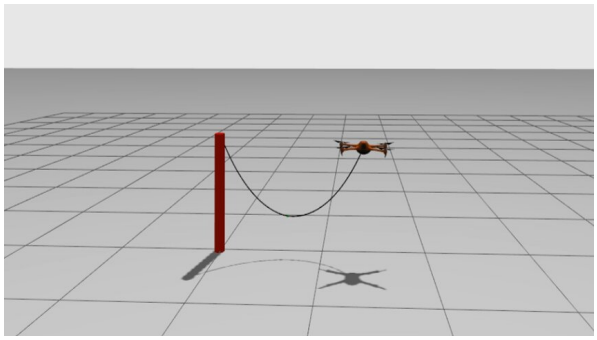

(a) Image showing the shape manipulation of a cable with a quadrotor

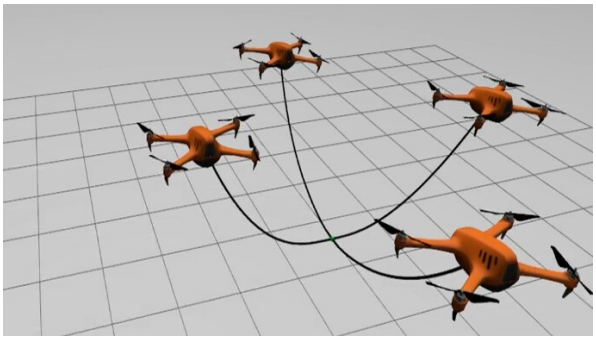

(b) Image showing the complete system configuration

Figure 5.23: Image showing the cable being tested with single and multiple multi-rotors, used for the development of controllers

the ROS2 bridge node inside the ROS 2 bridge block acting as a two way communication path. This also helps to close the loop with sensor data from the simulation model like force sensor, pose etc to the system model in Matlab/Simulink. Although the message format between Matlab/Simulink and Ignition are different, there is a message map inside ROS 2 bridge node which makes it possible. Further, the addition of ROS 2 enables to have the low level controller to be used from existing open source packages like Aerostack 2 etc. This also enables modularity of the framework to changes components of the framework independently.

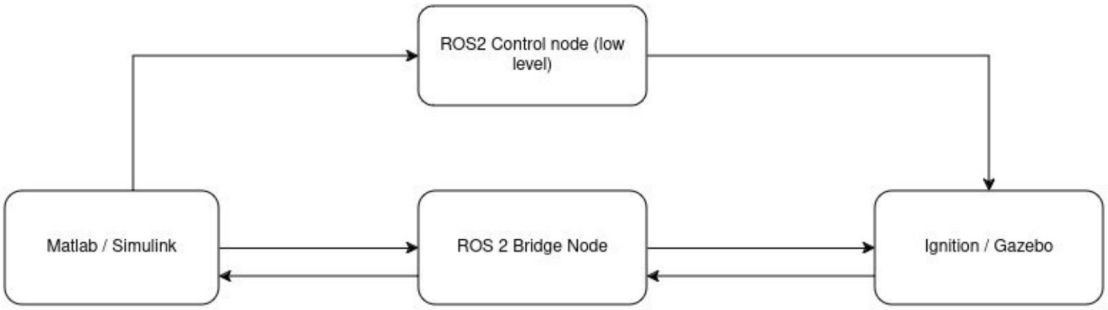

Figure 5.24: Block diagram of the software framework

5.4 Summary

This section evaluates all the above discussed simulation models used to test the system. The most suitable model is found based on the evaluation criteria.

Evaluation Criteria	**Sampling based Energy Optimisation Model**	**Elasto-Flexible Model**	**Physics Simulator Model**
Pros	Provides stable equilibrium	Dynamic model	Physics-based and realistic along with being dynamic
Cons	Computationally inefficient, exhaustive search and sampling-based	Larger model mismatch, arbitrary tuning of parameters and stability problems	High environment setup time
Assumptions	Quasi-staticity	Lumped parameters of the cable	cable as combination of many rigid bodies
Usefulness of model for control purposes	cannot be used for model based controllers as there is no closed form solution	algebraic expression of forces used to get feasible trajectories by exploiting system property (differential flatness)	Ability to close the feedback loop with sensor information (eg:- force, position etc)

Table 5.2: Summary of all the methods used in simulation

6 Conclusion & Recommendations

The research questions for the thesis were answered by developing the system from scratch for the targeted application and validating them.

6.1 Conclusion

6.1.1 Consider a system composed of multiple multirotors connected through deformable passive elements, such as cables. Identify a suitable model for such a system. The steps will be: a study of the literature on cable-connected aerial robotic systems; identification of a suitable model (simple yet realistic); and validation of the model

A detailed literature survey was conducted in deformable object manipulation by aerial robots. The deformable linear object (DLO) type of modelling were narrowed down due to it's simplicity. Then different methods for DLO type of modeling were studied and compared. A simple one parameter model of catenary curve is selected as the prefereed DLO model. A detailed lieterature survey for catenary type of modeling was conducted and show as a tabular column for the applications used and the control and planning methods with the catenary model. Then, a system model of the deformable net based on the catenaries were formulated, the modelling assumptions and hypothesis were validated with real world experiments of the cables. The metrics for the experiments were analysed and the modeling hypothesis was verified. In this way, a suitable model for the system is formed.

6.1.2 How to simulate such a system? Identify challenges, pros, and cons.

A simulation framework is built to test the developed system model. The simulation framework needed a second model representing the system. The identification and development of this second model was very challenging because there was no open source or available model that can be used. Due to this an energy optimisation method was developed which was computationally intensive and could not be used. Then, an available elasto-fleible model in the group was modified and used, unfortunately the model mismatch was high to be used for simulation purposes. Hence, a physics simulator is used by building the model and tuning the model for performance in the physics simulator. The detailed comparison between the three methods is given in table 5.2. Finally the physics simulator model was chosen due to it's modularity, pjysical properties with realistic nature and possibility of having the dynamics. It was very challenging to build this framework entirely from scratch as it involved a lot of software development and work around to make it work.

6.2 Recommendations

One of the main problems in using the system model was finding the point that connects all the cables together. I made many attempts to derive an analytical expression for finding this point. The methods I developed had a higher range of error above 10% . The methods i tried were using geometrical reasoning and using force balance equations to derive an algebraic expression. In the future, optimisation based method needs to be developed to find this cable connection point based on the force balance equations.

While simulating the model, the potential energy based optimisation method worked. The work in the direction was stopped due to computational intensity and work in that direction may not yield a viable result in the available time. In future, the optimisation can be refined using differential gradient based search instead o sampling based optimisation. Generally, gradient based optimisation are faster and this line of work can be continued and this can lead to energy based control for the system. This will enable co-ordinate free way of modeling and controlling the system.

Since the system moves in a quasi-static way, the static equilibrium always exists. In future, conditions for static equilibrium can be derived and this will make the system maintain a pose and shape in the presence of external disturbances like wind, water etc by rejecting these disturbances. The knowledge of static equilibrium of the model will be useful to have a robust planner or controller for the system in the presence of external disturbance.

Finally, the most important part is to tract the system to a desirable configuration with simultaneous pose and shape control. I started making attempts at implementing an admittance controller for the system unfortunately there was not enough time to finish it. In the future, it would be interesting to see how these controllers work on the system and which type of control methodology is most suitable to tract the system, like reactive controllers or model based controllers.

Bibliography

[1] Vishal Abhishek, Vaibhav Srivastava and Ranjan Mukherjee. 'Towards a heterogeneous cable-connected team of UAVs for aerial manipulation'. In: *2021 American Control Conference (ACC)*. IEEE. 2021, pp. 54–59.

[2] Satoko Abiko et al. 'Obstacle avoidance flight and shape estimation using catenary curve for manipulation of a cable hanged by aerial robots'. In: *2017 IEEE International Conference on Robotics and Biomimetics (ROBIO)*. IEEE. 2017, pp. 2099–2104.

[3] Federico Augugliaro et al. 'Knot-tying with flying machines for aerial construction'. In: *2015 IEEE/RSJ International Conference on Intelligent Robots and Systems (IROS)*. IEEE. 2015, pp. 5917–5922.

[4] Tomas Baca et al. 'The MRS UAV system: Pushing the frontiers of reproducible research, real-world deployment, and education with autonomous unmanned aerial vehicles'. In: *Journal of Intelligent & Robotic Systems* 102.1 (2021), p. 26.

[5] Stamatina C Barakou, Costas S Tzafestas and Kimon P Valavanis. 'A Survey of Modeling and Control Approaches for Cooperative Aerial Manipulation'. In: *2024 International Conference on Unmanned Aircraft Systems (ICUAS)*. IEEE. 2024, pp. 610–617.

[6] Stamatina C Barakou, Costas S Tzafestas and Kimon P Valavanis. 'Real-time applicable cooperative aerial manipulation: A survey'. In: *2023 International Conference on Unmanned Aircraft Systems (ICUAS)*. IEEE. 2023, pp. 634–643.

[7] Andrea Borgese et al. 'Tether-based localization for cooperative ground and aerial vehicles'. In: *IEEE Robotics and Automation Letters* 7.3 (2022), pp. 8162–8169.

[8] Samir Bouabdallah and Roland Siegwart. 'Full control of a quadrotor'. In: *2007 IEEE/RSJ international conference on intelligent robots and systems*. Ieee. 2007, pp. 153–158.

[9] Gustavo A Cardona et al. 'Adaptive control for cooperative aerial transportation using catenary robots'. In: *2021 Aerial Robotic Systems Physically Interacting with the Environment (AIRPHARO)*. IEEE. 2021, pp. 1–8.

[10] Dimitris Chaikalis et al. 'Design, modelling, localization, and control for fire-fighting aerial vehicles'. In: *2022 30th Mediterranean Conference on Control and Automation (MED)*. IEEE. 2022, pp. 432–437.

[11] Ryan Cotsakis, David St-Onge and Giovanni Beltrame. 'Decentralized collaborative transport of fabrics using micro-UAVs'. In: *2019 International Conference on Robotics and Automation (ICRA)*. IEEE. 2019, pp. 7734–7740.

[12] Diego S DAntonio, Subhrajit Bhattacharya and David Saldaña. 'Forming and controlling hitches in midair using aerial robots'. In: *2023 IEEE International Conference on Robotics and Automation (ICRA)*. IEEE. 2023, pp. 1270–1276.

[13] Diego S Dantonio, Gustavo A Cardona and David Saldana. 'The catenary robot: Design and control of a cable propelled by two quadrotors'. In: *IEEE Robotics and Automation Letters* 6.2 (2021), pp. 3857–3863.

[14] Diego S DAntonio and David Saldana. 'Folding knots using a team of aerial robots'. In: *2022 IEEE/RSJ International Conference on Intelligent Robots and Systems (IROS)*. IEEE. 2022, pp. 3372–3377.

[15] Diego S DAntonio and David Saldaña. 'Folding Knots Using a Team of Aerial Robots'. In: *2022 IEEE/RSJ International Conference on Intelligent Robots and Systems (IROS)*. IEEE. 2022, pp. 3372–3377.

[16] Georgios Darivianakis et al. 'Hybrid predictive control for aerial robotic physical interaction towards inspection operations'. In: *2014 IEEE international conference on robotics and automation (ICRA)*. IEEE. 2014, pp. 53–58.

[17] Subhranil De. 'The Curious Case of the Double Catenary'. In: *Mathematics Magazine* 95.3 (2022), pp. 220–229.

[18] Peter Dear. *Discipline and experience: The mathematical way in the scientific revolution*. University of Chicago Press, 2009.

[19] Sina Doroudgar. 'Static and dynamic modeling and simulation of the umbilical cable in a tethered unmanned aerial system'. In: (2016).

[20] Juliette Drupt et al. 'Inertial-measurement-based catenary shape estimation of underwater cables for tethered robots'. In: *2022 IEEE/RSJ International Conference on Intelligent Robots and Systems (IROS)*. IEEE. 2022, pp. 6867–6872.

[21] Martin Filliung et al. 'An Augmented Catenary Model for Underwater Tethered Robots'. In: *IEEE International Conference on Robotics and Automation (ICRA 2024)*. 2024.

[22] Francesco Forte et al. 'On the control of an aerial manipulator interacting with the environment'. In: *2014 IEEE International Conference on Robotics and Automation (ICRA)*. IEEE. 2014, pp. 4487–4492.

[23] G.Apostolo. *Breguet-Richet no. 1 gyroplane*. https://artsandculture.google.com/asset/breguet-richet-no-1-gyroplane-louis-breguet/JwH1CFNu44563Q?hl=en. Accessed: 2024-08-07. 1984.

[24] G.Apostolo. *De Bothezat*. http://www.aviastar.org/helicopters_eng/bothezat.php. Accessed: 2024-08-14. 1984.

[25] Chiara Gabellieri and Antonio Franchi. 'Differential Flatness and Manipulation of Elasto-flexible Cables Carried by Aerial Robots in a Possibly Viscous Environment'. In: *2023 International Conference on Unmanned Aircraft Systems (ICUAS)*. IEEE. 2023, pp. 963–968.

[26] Brendan Galea and Paul G Kry. 'Tethered flight control of a small quadrotor robot for stippling'. In: *2017 IEEE/RSJ International Conference on Intelligent Robots and Systems (IROS)*. IEEE. 2017, pp. 1713–1718.

[27] Farhad A Goodarzi, Daewon Lee and Taeyoung Lee. 'Geometric control of a quadrotor UAV transporting a payload connected via flexible cable'. In: *International Journal of Control, Automation and Systems* 13 (2015), pp. 1486–1498.

[28] Seiga Kiribayashi, Kaede Yakushigawa and Keiji Nagatani. 'Position estimation of tethered micro unmanned aerial vehicle by observing the slack tether'. In: *2017 IEEE International Symposium on Safety, Security and Rescue Robotics (SSRR)*. IEEE. 2017, pp. 159–165.

[29] Denis Kotarski et al. 'Concept of a modular multirotor heavy lift unmanned aerial vehicle platform'. In: *Aerospace* 10.6 (2023), p. 528.

[30] Prasanth Kotaru, Guofan Wu and Koushil Sreenath. 'Differential-flatness and control of quadrotor (s) with a payload suspended through flexible cable (s)'. In: *2018 Indian Control Conference (ICC)*. IEEE. 2018, pp. 352–357.

[31] Matheus Laranjeira, Claire Dune and Vincent Hugel. 'Catenary-based visual servoing for tether shape control between underwater vehicles'. In: *Ocean Engineering* 200 (2020), p. 107018.

[32] Matheus Laranjeira, Claire Dune and Vincent Hugel. 'Catenary-based visual servoing for tethered robots'. In: *2017 IEEE International Conference on Robotics and Automation (ICRA)*. IEEE. 2017, pp. 732–738.

[33] Rogerio R Lima and Guilherme AS Pereira. 'A multi-model framework for tether-based drone localization'. In: *Journal of Intelligent & Robotic Systems* 108.2 (2023), p. 20.

[34] Rogerio R Lima and Guilherme AS Pereira. 'On the development of a tether-based drone localization system'. In: *2021 International Conference on Unmanned Aircraft Systems (ICUAS)*. IEEE. 2021, pp. 195–201.

[35] Chen Liu, Li Ding and JiaHui Gu. 'Dynamic Modeling and Motion Stability Analysis of Tethered UAV'. In: *2021 5th International Conference on Robotics and Automation Sciences (ICRAS)*. IEEE. 2021, pp. 106–110.

[36] Krossblade Aerospace Systems LLC. *History of Quadcopters and other Multirotors*. https://www.krossblade.com/history-of-quadcopters-and-multirotors. Accessed: 2024-08-06. 2022.

[37] Simón Martinez-Rozas et al. 'Optimization-based trajectory planning for tethered aerial robots'. In: *2021 IEEE International Conference on Robotics and Automation (ICRA)*. IEEE. 2021, pp. 362–368.

[38] Ricardo Martins and Meysam Basiri. 'Tension Estimation and Localization for a Tethered Micro Aerial Robot'. In: *arXiv preprint arXiv:2302.03551* (2023).

[39] Anibal Ollero et al. 'Past, present, and future of aerial robotic manipulators'. In: *IEEE Transactions on Robotics* 38.1 (2021), pp. 626–645.

[40] Sigitas Rimkus, Tuhin Das and Ranjan Mukherjee. 'Stability analysis of a tethered airfoil'. In: *2013 American Control Conference*. IEEE. 2013, pp. 5601–5606.

[41] Robin Ritz et al. 'Cooperative quadrocopter ball throwing and catching'. In: *2012 IEEE/RSJ International Conference on Intelligent Robots and Systems*. IEEE. 2012, pp. 4972–4978.

[42] Minghe Shan, Jian Guo and Eberhard Gill. 'Deployment dynamics of tethered-net for space debris removal'. In: *Acta Astronautica* 132 (2017), pp. 293–302.

[43] Yaolei Shen, Chiara Gabellieri and Antonio Franchi. 'Aerial Robots Carrying Flexible Cables: Dynamic Shape Optimal Control via Spectral Method Model'. In: *arXiv preprint arXiv:2403.17565* (2024).

[44] Lev Smolentsev, Alexandre Krupa and François Chaumette. 'Shape visual servoing of a tether cable from parabolic features'. In: *2023 IEEE International Conference on Robotics and Automation (ICRA)*. IEEE. 2023, pp. 734–740.

[45] Marios-Nektarios Stamatopoulos et al. 'Combined Aerial Cooperative Tethered Carrying and Path Planning for Quadrotors in Confined Environments'. In: *2023 31st Mediterranean Conference on Control and Automation (MED)*. IEEE. 2023, pp. 364–369.

[46] Miguel Such et al. 'An approach based on the catenary equation to deal with static analysis of three dimensional cable structures'. In: *Engineering structures* 31.9 (2009), pp. 2162–2170.

[47] Masaya Suzuki et al. 'Liquid feeding system using cooperative towing by multiple drones2nd Report: Position estimation of each drones based on catenary theory and tensile force of tube'. In: *2018 IEEE International Conference on Industrial Technology (ICIT)*. IEEE. 2018, pp. 217–222.

[48] Kurt A Talke, Mauricio De Oliveira and Thomas Bewley. 'Catenary tether shape analysis for a UAV-USV team'. In: *2018 IEEE/RSJ International Conference on Intelligent Robots and Systems (IROS)*. IEEE. 2018, pp. 7803–7809.

[49] Te Tang et al. 'Robotic manipulation of deformable objects by tangent space mapping and non-rigid registration'. In: *2016 IEEE/RSJ International Conference on Intelligent Robots and Systems (IROS)*. IEEE. 2016, pp. 2689–2696.

[50] Inc The MathWorks. *Documentation Hyperbolic Cosine function*. Accessed: 2024-08-22. 2024. URL: https://nl.mathworks.com/help/matlab/ref/cosh.html.

[51] Carlos G Valerio, Eduardo S Espinoza and Rogelio Lozano. 'Control and cable deployment of a tethered PVTOL aircraft'. In: *2021 18th International Conference on Electrical Engineering, Computing Science and Automatic Control (CCE)*. IEEE. 2021, pp. 1–6.

[52] Zixing Wang and Ahmed H Qureshi. 'DeRi-Bot: Learning to collaboratively manipulate rigid objects via deformable objects'. In: *IEEE Robotics and Automation Letters* (2023).

[53] Xuesu Xiao, Jan Dufek and Robin Murphy. 'Benchmarking tether-based UAV motion primitives'. In: *2019 IEEE International Symposium on Safety, Security, and Rescue Robotics (SSRR)*. IEEE. 2019, pp. 51–55.

[54] Xuesu Xiao et al. 'Indoor UAV Localization Using a Tether'. In: *2018 IEEE International Symposium on Safety, Security, and Rescue Robotics (SSRR)*. 2018, pp. 1–6. DOI: 10.1109/SSRR.2018.8468627.

[55] Hyunsoo Yang et al. 'Modeling and control of multiple aerial-ground manipulator system (magmas) with load flexibility'. In: *2018 IEEE/RSJ International Conference on Intelligent Robots and Systems (IROS)*. IEEE. 2018, pp. 1–8.

[56] Sun Zhaole, Jihong Zhu and Robert B Fisher. 'DexDLO: Learning Goal-Conditioned Dexterous Policy for Dynamic Manipulation of Deformable Linear Objects'. In: *2024 IEEE International Conference on Robotics and Automation (ICRA)*. IEEE. 2024, pp. 16009–16015.

7 Appendix

7.1 Water Interaction in Gazebo

https://github.com/osrf/vrx

https://github.com/srmainwaring/asv_wave_sim

https://github.com/uuvsimulator/uuv_simulator/issues/375

Water simulation USV , with waste collection - https://ieeexplore.ieee.org/stamp/stamp.jsp?arnumber=9641589&casa_token=aC28iyH_c7EAAAAA:Jnv76LydIo46a6FKfj7wROm2D_OFwa2DdZPB1cRnbUKcm2emdI7QtRmHiTaaAw

Gazebo answers for surface water dynamics - https://community.gazebosim.org/t/simulate-surface-waves-and-marine-vehicle-dynamics/1268

Gazebo hydro dynamics plugin - https://classic.gazebosim.org/tutorials?tut=hydrodynamics&cat=physics

Gazebo fluid dynamics - https://classic.gazebosim.org/tutorials?tut=fluids&cat=physics

Look at the first video on SDF format 1.7 semantics - https://classic.gazebosim.org/blog.html

7.1.1 Fire hose model

https://github.com/osrf/drcsim/blob/master/drcsim_model_resources/gazebo_models/fire_hose/model.sdf

7.1.2 RotorS

RotorS - https://github.com/ethz-asl/rotors_simulator/wiki Interfacing RotorS through MATLAB - https://github.com/ethz-asl/rotors_simulator/wiki/Interfacing-RotorS-through-Matlab#Examples-Controller

CrazyS - https://github.com/gsilano/CrazyS and https://giuseppesilano.net/publications/med18.pdf

7.1.3 Matlab/Simulink and Gazebo Interface Co-simulation

https://nl.mathworks.com/matlabcentral/answers/859380-control-uav-in-gazebo-with-simulink

connectivity with simulators - https://nl.mathworks.com/help/ros/connectivity-to-ros-enabled-simulators.html

7.1.4 Obi rope

Official forum - http://obi.virtualmethodstudio.com/forum/archive/index.php?thread-1132.html

General info from the studio - http://obi.virtualmethodstudio.com/

EXtended position based dynamics - https://carmencincotti.com/2022-08-08/xpbd-extended-position-based-dynamics/

Quadrotor simulator in Unity - https://github.com/udacity/RoboND-QuadRotor-Unity-Simulator

https://carmencincotti.com/2022-09-05/the-most-performant-bending-constraint-of-xpbd/

7.1.5 Crazyfly simulators

https://www.bitcraze.io/2021/12/simulation-possibilities/

7.1.6 Simulink crash problems

working method - https://nl.mathworks.com/matlabcentral/answers/1454674-why-does-matlab-crash-on-linux-with-inconsistency-detected-by-ld-so-elf-dl-tls-c-597-_dl_allo

similar question - https://nl.mathworks.com/matlabcentral/answers/1567188-simulink-crash-in-ubuntu-20-04

https://nl.mathworks.com/support/bugreports/2632298

7.1.7 Ignition vs Gazebo

https://www.allisonthackston.com/articles/ignition-vs-gazebo.html

Gazebo tested crazyfly both in Gazebo and ignition - https://github.com/knmcguire/crazyflie_models

https://forum.bitcraze.io/viewtopic.php?t=4886

7.1.8 SDF tutorial

1. https://sdformat.org/tutorials
2. https://github.com/gazebosim/sdf_tutorials
3. https://flow.mov.ai/docs/overview

7.1.9 Gazebo-simulink sim multiple sessions

https://nl.mathworks.com/help/robotics/ug/run-and-connect-to-multiple-gazebo-sessions-from-simulink.html

https://nl.mathworks.com/help/robotics/ug/configure-gazebo-for-co-simulation-of-manipulator.html

https://nl.mathworks.com/help/robotics/ug/perform-co-simulation-between-simulink-and-gazebo.html#PerformCoSimulationBetweenSimulinkAndGazeboExam2

https://nl.mathworks.com/help/robotics/ug/control-a-differential-drive-robot-in-simulink-and-gazebo.html

7.2 Literature survey

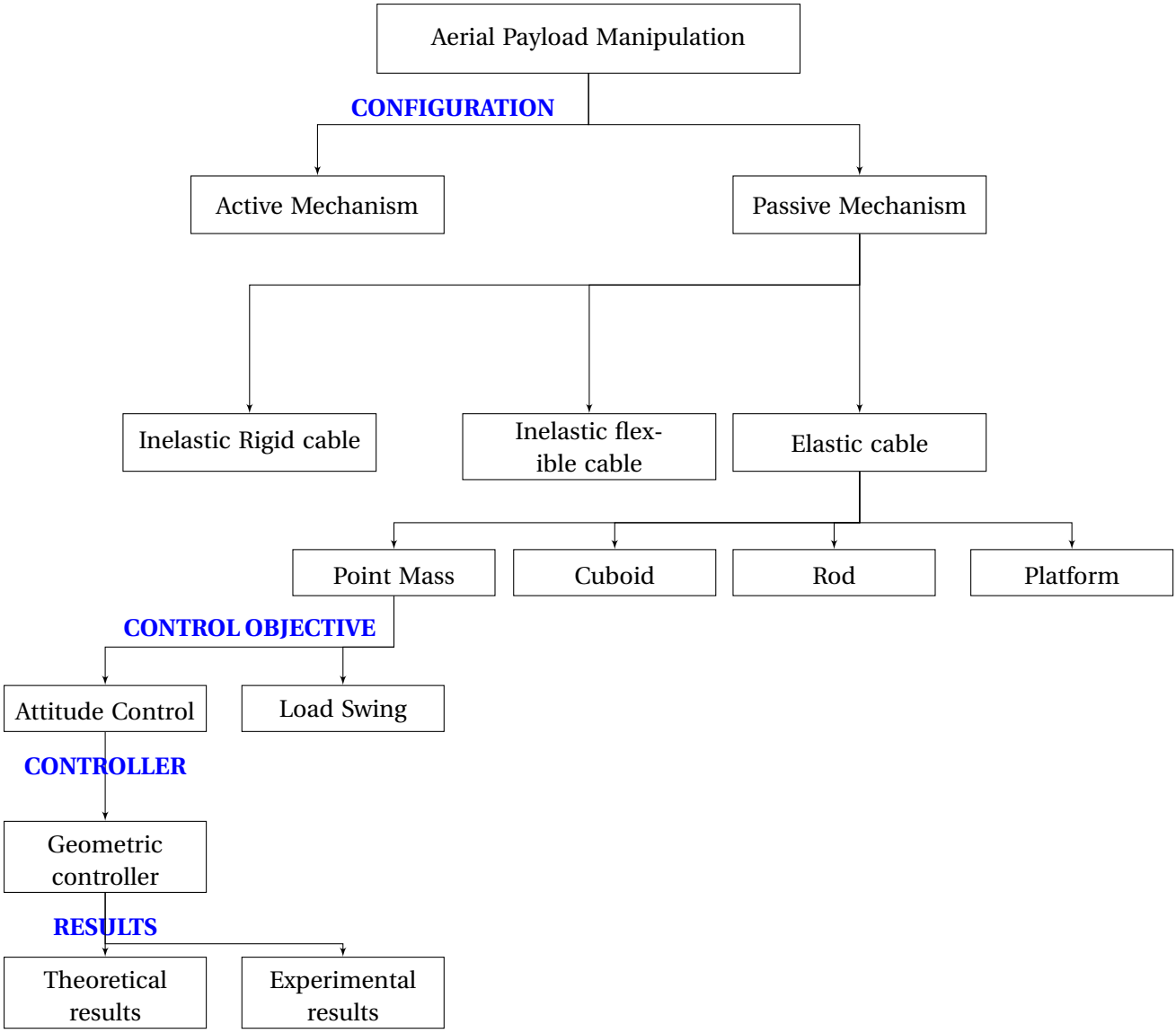

Figure 7.1: Block Diagram of Literature Survey

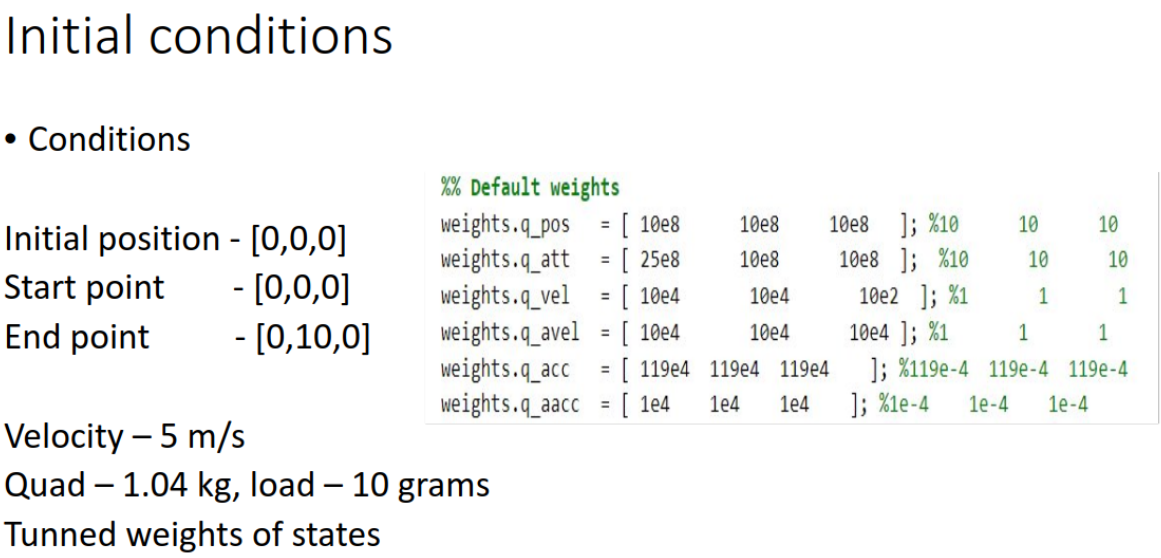

Figure 7.2: Conditions and tuning of NMPC controller

7.3 NMPC controller for cable load position tracking

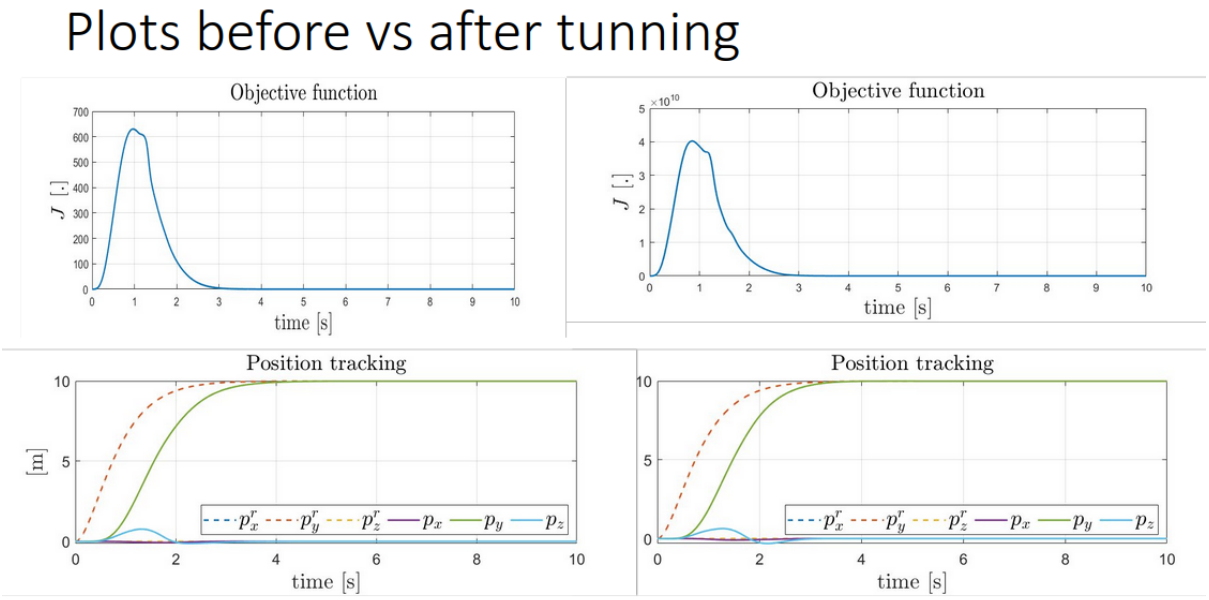

Figure 7.3: Object function and load position tracking